

1 Reviewer 1 Comments and Response:

Formatted: Font color: Text 1

2

3 **Compared to the previous version, this updated version of the manuscript has**
4 **improved a lot. Although I should note that not all suggestions raised have been**
5 **accounted for. However, the performed work, results and conclusions are well**
6 **presented.**

Formatted: Font: 10 pt, Bold, Font color: Text 1

7 **There is only one final detail that I would like to see altered before I feel the**
8 **manuscript is ready for publication. At multiple places (both in the abstract and**
9 **conclusion) the authors talk about 1100 of radar precipitation observations.**
10 **However, this is just 46 days of data. At another location details are provided that**
11 **actually 400 of the 1100 hours contained precipitation. I would therefore suggest**
12 **that the authors alter the 1100 into 400 hours of precipitation**

13

14 We thank the reviewer for the above comments. We have updated the necessary changes throughout
15 the manuscript to properly reflect the correct number of days and precipitation amounts.

16

17

18

19

20

21

22

23

24

25

26

27

28

29

30

31

32

33

34

35

36

37
38
39
40
41
42
43
44
45
46
47
48
49
50
51
52
53
54
55
56
57
58
59
60
61
62
63
64
65
66
67
68
69
70
71
72
73

Reviewer 2 Comments and Responses:

The paper could provide a long-term verification of dual-pol QPE algorithms which is relevant for hydrology. The authors stress that they focus on the range effect but this is in contradiction with the extended list of objectives in the introduction and the limited amount of results related to range in the conclusions

Formatted: Font: 12 pt, Bold

We appreciate this comment. We have added discussion in the conclusions to elaborate upon this aspect. We also added elaboration in the list of objects (near line 79 on page 3) to emphasize the range effect.

The number of data is limited. Why only one year? Why only 46 days of precipitation are available when the normal is around 100 days?

Formatted: Font: 12 pt, Bold

We chose a random year for the analyses to be conducted, we elaborated that 100 days have 'measurable' rainfall (i.e., greater than trace) whereas 50 days have greater than 0.5mm in of rainfall. Therefore, the 46 days chosen / analyzed falls near the average amount of days with appreciable rainfall.

The conclusions are short and do not summarize clearly the main findings (i.e. the algorithm's relative performance in function of the range). A proper discussion on the validity and possible cause of the different results is missing

Formatted: Font: 12 pt, Bold

Thank you for this comment. We have expanded upon the conclusions which were lacking in wrapping the paper up.

The information on the data and their quality is still limited while it seems some observation errors affect the results. Which type of quality control is effectively performed by WDSS-II on the radar data? Why not using the one-hour precipitation product of NOAA as reference? Why using the Mesonet network when the higher resolution CoCoRaHS is considered as better by the authors? The data selection criteria and choice of statistics are not sufficiently discussed.

Formatted: Font: 12 pt, Bold

We have added a more detailed description of the quality controlled techniques implemented, which would mitigate large errors in QPE from various modules within the WDSS-II framework. We did not consider using the DP rate as a reference, as that is more of a heuristic algorithm that blends multiple different algorithms together (it is difficult to determine whether they implement R(KDP), R(Z,ZDR), etc.) without doing a deep analysis of the radar parameter values as well as the particular algorithm implemented at each time. Furthermore, it is difficult to determine whether each of the 3 radar locations implement the same sort of dual-pol radar equation at the same times. Lastly, We implemented the Mesonet data due to the timing in which the current study was conducted. The authors have follow-up studies which utilize CoCoRaHS, HADS, MADIS, and other gauge locations.

74 In Figure 2, the results vary a lot between the algorithm's and the radars making
75 interpretations difficult. I am surprised by the bad performance of KDP (did you check the
76 cause visually?). The tentative explanations of radar issues for specific gauges (e.g. bright
77 band effect) are not robust. In Figure 3-8, only the overall best and worst algorithm's are
78 shown, which is too limited (I would present the best of each type). It is often unclear for
79 which algorithm an interpretation is valid.

Formatted: Font: 12 pt, Bold

80 We thank the reviewer for these comments. After checking visually, bright-banding were present in
81 several cases, but the w2qcndp as well as w2qcnn algorithms *should* have handled them effectively
82 (cases slip through, of course). We have addressed this within the text which is primarily the result of
83 the large biases observed in spite of larger distance from the radar. The algorithms represented via
84 Figures 3-8 are labeled within the caption and represent the best-performing R(Z,ZDR) and worst
85 performing R(ZDR,KDP) algorithms. This helps to highlight differences between the algorithms not only
86 between the warm, but also the cool season.

87 The results of similar studies (including from the authors) are not properly reviewed. Is there
88 a connection with your recently submitted article on X-Band?

Formatted: Font: 12 pt, Bold

89 We have seen similarities with the superiority of R(Z,ZDR) algorithms over R(ZDR,KDP) or R(KDP). We
90 did, as well, see superiority with the R(Z)-Convective equation as well.

91 The description of the statistical analyses needs to be much more clear and precise (proper
92 definition and interpretation, thresholds used for zeros, selection of hit only data)

Formatted: Font: 12 pt, Bold

93 We appreciate this comment, and have elaborated on the definition of thresholds and hit only at the
94 end of the statistical analyses section in which more than 2 tips were needed for calculations to be
95 implemented.

96 The new title sounds a bit odd to me

Formatted: Font: 12 pt, Bold

97 We have changed the title of the article to make it flow better.

98 The abstract has not been improved as suggested and is not consistent with the conclusions.

Formatted: Font: 12 pt, Bold

99 We appreciate this reviewer comment, and have expanded on the abstract to better reflect the
100 conclusion, make it easier to read, and fixed some spelling errors.

101 The comments have not been taken into account. There is still part of the methodology in the
102 "results" section.

Formatted: Font: 12 pt, Bold

103 We thank the reviewer for this comment, and we have moved text to/from the methodology and results
104 section to better reflect the text within each section.

105 No significant efforts have been made to improve the text structure, terminology and style.
106 There are annoying editing errors at this stage (e.g. a repeated sentence on line 212)

Formatted: Font: 12 pt, Bold

107 We have moved text around throughout the methodology and results to create a better-flowing
108 manuscript.

109 **Some definitions are still incorrect or imprecise**

Formatted: Font: 12 pt, Bold

110 The authors thank the reviewer for this comment. We have gone through the text and ensured accuracy
111 in the definition and spelling of each acronym.

112 **The results section is still not clear nor concise. There are too much points in Figure 2. There**
113 **are too much plots in the figures. I would show only NMB, NME, PoFD, PoD. Paragraphs over**
114 **the different radars could be combined. What is exactly on figures 2-8 : best at each point**
115 **(your response) or only R(Z,ZDR) (figure caption)?**

Formatted: Font: 12 pt, Bold

116 We have utilized only the best algorithm from the set of R(Z,ZDR) equations and the worst algorithm
117 from the set of R(ZDR,KDP) equations as these consistently showed to be the best and worst,
118 respectively. We have implemented the data from each of the statistical analyses to better represent
119 the performance of each algorithm at each radar. Some results would not have been accounted for or
120 even could have been completely missed without some of the statistical measures analyzed in this
121 fashion.

122 **The number and quality of the references are acceptable but they are often cited for**
123 **anecdotal reasons (e.g. Figueras et al. on line 381). They are best used for discussion in the**
124 **introduction and conclusions sections.**

Formatted: Font: 12 pt, Bold

125 We have altered our references and moved them around to be more appropriate for the current study.

126

127

128

129

130

131

132

133

134

135

136

137

138

139

140

141

142

143

144
145
146
147
148
149
150
151
152
153
154
155
156
157
158
159
160
161
162
163
164
165
166
167
168
169
170
171
172
173
174

RANGE AS A FUNCTION OF DUAL-POLARIZED QUANTITATIVE PRECIPITATION ESTIMATION AS A FUNCTION OF RANGE

Micheal J. Simpson¹ and Neil I. Fox²

¹University of Missouri, School of Natural Resources, Water Resources Program, Department of Soil, Environmental, and Atmospheric Sciences, 203-T ABNR Building, Columbia, Missouri, USA, 65211. Tel: +001 4053256459 Email: mjs5h7@mail.missouri.edu

³Cooperative Institute of Mesoscale Meteorological Studies, University of Oklahoma, National Severe Storms Laboratory, Norman, Oklahoma. Tel: +001 4053256459. Email: micheal.simpson@noaa.gov

²University of Missouri, School of Natural Resources, Water Resources Program, Department of Soil, Environmental, and Atmospheric Sciences, 332 ABNR Building, Columbia, Missouri, USA, 65211. Tel: +001 5738822144 Email: FoxN@Missouri.edu

Correspondence to: Micheal J. Simpson (micheal.simpson@noaa.gov)

Abstract. Since the advent of dual-polarization radar technology, many studies have been conducted to determine the extent to which the differential reflectivity (ZDR) and specific differential phase shift (KDP) add benefits to estimating rain rates (R) compared to reflectivity (Z) alone. It has been previously noted that this new technology provides significant improvement to rain rate estimation, primarily for ranges within 125 km of the radar. Beyond this range, it is unclear as to whether the National Weather Service conventional R(Z)-Convective algorithm is superior, as little research has investigated radar precipitation estimate performance at larger ranges. The current study investigates the performance of three radars, St. Louis (KLSX), Kansas City (KEAX), and Springfield (KSGF), MO, with 15 tipping bucket gauges serving as ground-truth to the radars. With over 300 hours of precipitation data were analyzed for the current study, it was found that, in general, performance degraded with range beyond,

Formatted: Font: (Default) Times New Roman

Formatted: Normal, No bullets or numbering

Formatted: Font: (Default) Times New Roman

Formatted: Font: (Default) Times New Roman

Formatted: Font: (Default) Times New Roman

175 approximately, 150 km from each of the radars. Probability of detection in addition to bias values
176 decreased, while the false alarm rates increased as range increased. Bright-band contamination was
177 observed to play a potential role as large increases in the absolute bias and overall error values near 120
178 km for the cool season, and 150 km in the warm season. Furthermore, upwards of 60% of the total error
179 was due to precipitation falsely estimated, while 20% of the total error was due to missed precipitation.
180 Correlation coefficient values increased by as much as 0.4 when these instances were removed from the
181 analyses (i.e., hits only). Overall, due to the lowest normalized standard error of less than 1.0, a National
182 Severe Storms Laboratory (NSSL) R(Z,ZDR) equation was determined to be the most robust, while a
183 R(ZDR,KDP) algorithm recorded NSE values as much as 5. The addition of dual-polarized technology
184 was shown to better estimate quantitative precipitation estimates than the conventional equation. The
185 analyses further our understanding in the strengths and limitations of the Next Generation Radar system
186 overall, and from a seasonal perspective.

187
188 **Abstract.** Since the advent of dual-polarized radar technology, many studies have been conducted to
189 determine the extent to which the differential reflectivity (ZDR) and specific differential phase shift
190 (KDP) add benefits to estimating rain rates (R) compared to reflectivity (Z). It has been previously noted
191 that this new technology provides significant improvement to rain rate estimation, but only for ranges
192 within 125 km from of the radar. Beyond this range, it is unclear as to whether the National Weather
193 Service conventional R(Z)-Convective algorithm is superior, as little research has investigated radar
194 precipitation estimate performance at large ranges. The current study investigates the performance of
195 three radars, St. Louis (KLSX), Kansas City (KEAX), and Springfield (KSGF), MO, with respect to
196 range, with 15 terrestrial based tipping bucket gauges served serving as ground truth to the radars. Over
197 1100-300 hours of precipitation data were analyzed for the current study. It was found that, in general,
198 performance degraded with range beyond, approximately, 150 km from the radar. Probability of detection
199 in addition to bias values decreased, while the false alarm rates increased as range increased. Bright-

Formatted: Indent: Left: 0.5", No bullets or

Formatted: Highlight

Formatted: Highlight

band-contamination was observed to play a potential role as large increases in the absolute bias and overall error values near 120 km for the cool season, and 150 km in the warm season. Addition of dual-polarized technology was shown to better estimate quantitative precipitation estimates than the conventional equation. The analyses found further our understanding in the strengths and limitations of the Next-Generation Radar system overall, and from a seasonal perspective.

1 Introduction

In 2012, the National Weather Service (NWS) began upgrading the Next Generation Radar (NEXRAD) system from single- to dual-polarization. The potential benefits of this upgrade were investigated by the National Severe Storms Laboratory (NSSL) and the Cooperative Institute for Mesoscale Meteorological Studies. These advantages include, but are not limited to, (1) significant improvement in radar rainfall estimation (Ryzhkov et al., 2005; Gourley et al., 2010) through better representation of precipitation shape (Brandes et al., 2002; Gorgucci et al., 2000, 2006), (2) discrimination between solid and liquid precipitation (Zrnich and Ryzhkov, 1996), allowing for better distinction between areas of heavy rain and hail (Park et al., 2009; Giangrande and Ryzhkov, 2008; Cunha et al., 2013), (3) identifying the melting layer position in the radar field (Straka et al., 2000; Park et al., 2009), and (4) calculating drop-size distributions retrieved from measurements of reflectivity (Z), differential reflectivity (ZDR), and specific differential phase shift (KDP) as opposed to using ground-based point located disdrometers (Zhang et al., 2001; Brandes et al., 2004; Anagnostou et al., 2008).

Rain rate retrieval by weather radars is an estimation based upon the dielectric properties of the hydrometeors encountered in the atmosphere. Therefore, there is no direct measurement of rainfall, and this inherently introduces error. However, dual-polarized radar technology allows for in-depth analyses on the microphysics of precipitation that single-polarization was incapable of conducting. In spite of this technology, conflicting studies report the benefits for quantitative precipitation estimation (QPE). For example, Gourley et al. (2010) and Cunha et al. (2015) reported that conventional $R(Z)$ algorithms have significantly better bias than algorithms containing ZDR and/or KDP , while others (e.g., Ryzhkov et al.,

225 2013; Simpson et al., 2016) report the opposite. This could be due, at least in part, to the fact that
226 hydrometeor types (e.g., rain versus hail) vary on spatial scales that cannot be easily resolved by even
227 densely gauged networks.

228 Multiple studies have found that the performance of radar rain rate estimates decrease as range
229 increases (Smith et al., 1996; Ryzhkov et al., 2003) which is caused, primarily, by degradation of beam
230 quality with range. Furthermore, the researchers also discuss how the probability of detection at larger
231 ranges decreases, as the radar beam overshoots shallow, stratiform precipitation, especially winter
232 precipitation. Bright-banding can also play a crucial role in significantly increasing the amount of
233 precipitation estimated by the radar, prompting many researchers to produce automated bright-band
234 detection algorithms (e.g., Zhang et al., 2008; Zhang and Qi, 2010).

235 Despite these overall disadvantages, studies have shown that radar rainrate algorithms seldom
236 exceed absolute errors on the order of 10 mm h⁻¹. However, many of these studies have looked at a small
237 sample of rain events (on the order of 10-50 hours) (Kitchen and Jackson, 1993; Smith et al., 1996;
238 Ryzhkov et al., 2003; Gourley et al., 2010; Cunha et al., 2013). Long-term performances of weather radar
239 are becoming more common in recent years as the availability of data becomes more abundant (e.g.,
240 Haylock et al., 2008; Goudenhoofdt and Delobbe, 2012; Fairman et al., 2015; Goudenhoofdt and
241 Delobbe, 2015). Additionally, few studies (e.g., Smith et al., 1996; Cunha et al., 2015; Simpson et al.,
242 2016) quantified QPE errors including the probability of detection and false alarm ratio. In order to gain a
243 better understanding of the performance of weather radars on rain rate estimates, more data must be
244 collected over a broad range of precipitation regimes in addition to an overall broader region of interest.

245 The overarching objective of the current study was to assess the performance of three different
246 radars within the state of Missouri at various ranges from the radar, using terrestrial-based tipping bucket
247 gauges as ground-truth data. Radar rain rate estimation algorithms include 55 algorithms encompassing
248 standard R(Z) relations as well as algorithms containing dual-polarization variables including differential
249 reflectivity (ZDR) and the specific differential phase shift (KDP). A rain rate echo classification

250 algorithm was also tested for performance in correctly identifying the suitable rain rate algorithm to
251 choose based on the Z, ZDR, and KDP radar fields. The current work expands upon that of Simpson et al.
252 (2016) such that a larger sample of data was analyzed (over 300 hours of rainfall data from forty-six
253 separate days in 2014) to encompass multiple different precipitation regimes for both summer and winter,
254 with several ground-truth tipping buckets to analyze the performance of three separate radars as a
255 function of range, and further expanding upon the effects of erroneous precipitation estimates on the
256 overall radar error. Objectives for this study included, (1) statistically analyze the performance of each
257 radar at various ranges (compared against the gauges), (2) compute (a) the amount of precipitation
258 incorrectly estimated by the radar (quantifying the probability of false detection) and (b) the amount of
259 precipitation incorrectly missed by the radar but measured by the rain gauge, (3) test the overall best radar
260 rain rate algorithm, and (4) perform objectives (1), (2), and (3) while the data is separated into warm and
261 cool seasons which have been shown to result in significantly different QPE's (Smith et al., 1996;
262 Ryzhkov et al., 2003; Cunha et al., 2015).

263 In 2012, the National Weather Service (NWS) began upgrading the Next-Generation Radar
264 (NEXRAD) system from single to dual polarization. The potential benefits of this upgrade were
265 investigated by the National Severe Storms Laboratory (NSSL) and the Cooperative Institute for
266 Mesoscale Meteorological Studies. These advantages include, but are not limited to, (1) significant
267 improvement in radar rainfall estimation (Ryzhkov et al., 2005; Gourley et al., 2010) through better
268 representation of precipitation shape (Brandes et al., 2002; Gorgucci et al., 2000, 2006), (2)
269 discrimination between solid and liquid precipitation (Zrnice and Ryzhkov, 1996), allowing for better
270 distinction between areas of heavy rain and hail (Park et al., 2009; Giangrande and Ryzhkov, 2008;
271 Cunha et al., 2013), (3) identifying the melting layer position in the radar field (Straka et al., 2000; Park
272 et al., 2009), and (4) calculating drop size distributions retrieved from measurements of reflectivity (Z),
273 differential reflectivity (ZDR), and specific differential phase shift (KDP) as opposed to using ground-
274 based point located disdrometers (Zhang et al., 2001; Brandes et al., 2004; Anagnostou et al., 2008).

275 Rain rate retrieval by weather radars is an estimation based upon the dielectric properties of the
276 hydrometeors encountered in the atmosphere. Therefore, there is no direct measurement of rainfall, and
277 this inherently introduces error. However, dual-polarized radar technology allows for in-depth analyses on
278 the microphysics of precipitation that single polarization was incapable of conducting. In spite of this
279 technology, conflicting studies report the benefits for quantitative precipitation estimation (QPE). For
280 example, Gourley et al. (2010) and Cunha et al. (2015) reported that conventional R(Z) algorithms have
281 significantly better bias than algorithms containing ZDR and/or KDP, while others (e.g., Ryzhkov et al.,
282 2013; Simpson et al., 2016) report the opposite. This could be due, at least in part, to the fact that
283 hydrometeor types (e.g., rain versus hail) vary on spatial scales that cannot be easily resolved by even
284 densely gauged networks.

285 Multiple studies have found that, in general, the performance of radar rain rate estimates decrease
286 as range increases (Smith et al., 1996; Ryzhkov et al., 2003) which is caused, primarily, by degradation of
287 beam quality and broadening of the beam with range. Furthermore, the researchers also discuss how the
288 probability of detection at larger ranges decreases, as the radar beam overshoots shallow, stratiform
289 precipitation, including winter storms. Bright banding can also play a crucial role in significantly
290 increasing the amount of precipitation estimated by the radar.

291 Despite these overall disadvantages, studies have shown that radar rain rate algorithms seldom
292 exceed absolute errors on the order of 10 mm h^{-1} . However, many of these studies have looked at a small
293 sample of rain events (on the order of 10-50 hours) (Kitchen and Jackson, 1993; Smith et al., 1996;
294 Ryzhkov et al., 2003; Gourley et al., 2010; Cunha et al., 2013). Long-term performances of weather radar
295 are becoming more common in recent years as the availability of data becomes more abundant (e.g.,
296 Haylock et al., 2008; Goudenhoofdt and Delobbe, 2012; Fairman et al., 2015; Goudenhoofdt and
297 Delobbe, 2015). Additionally, few studies (e.g., Smith et al., 1996; Cunha et al., 2015; Simpson et al.,
298 2016) quantified meteorologically significant measures including the probability of detection and false
299 alarm ratio. In order to get a better understanding of the performance of weather radars on rain rate

300 estimates, more data must be collected over a broad range of precipitation regimes in addition to an
301 overall broader region of interest.

302 The overarching objective of the current study was to assess the overall performance of three
303 different radars within the state of Missouri at various ranges from the radar, using terrestrial based
304 tipping bucket gauges as ground truth data. Radar rain rate estimation algorithms include 55 algorithms
305 encompassing standard R(Z) relations, in addition to and algorithms containing dual-polarization variables
306 including ZDR and KDP. A rain rate echo classification algorithm was also tested for performance in
307 correctly identifying the suitable rain rate algorithm to choose based on the Z, ZDR, and KDP radar
308 fields. The current work expands upon that of Simpson et al. (2016) such that a larger sample of data were
309 was analyzed (over 10300 hours of rainfall data from forty six separate days in 2014) to encompass
310 multiple different precipitation regimes for both summer and winter, with several ground truth tipping
311 buckets to analyze the performance of three separate radars as a function of range, and further expanding
312 upon the effects of erroneous precipitation estimates on the overall radar error. Objectives for this study
313 included, (1) statistically analyze the performance of each radar at various ranges (compared against the
314 terrestrial based gauges), (2) compute (a) the amount of precipitation incorrectly estimated by the radar
315 (quantifying the probability of false detection) and (b) the amount of precipitation incorrectly missed by
316 the radar but measured by the rain gauge, (3) test the overall best radar rain rate algorithm, and (4)
317 perform objectives (1), (2), and (3) while the data is separated into warm and cool seasons which have
318 been shown to result in significantly different QPE's (Smith et al., 1996; Ryzhkov et al., 2003; Cunha et
319 al., 2015).

320

321 2 Study area and methods

322 2.1 Study area

Formatted: Highlight

Formatted: Highlight

323 National Weather Service radars from St. Louis (KLSX), Kansas City (KEAX), and Springfield
324 (KSGF), MO are able to scan the majority of the state of Missouri. Because of this, the three
325 aforementioned radars were used to assess overall performance in estimating precipitation for this study.
326 Each radar covered a 200-km radius for which a different number of gauges were within the domain:
327 KLSX, KEAX, and KSGF covered 9, 8, and 5 gauges, respectively (Figure 1).

328 Missouri is characterized as a continental type of climate, marked by relatively strong seasonality.
329 Furthermore, Missouri is subject to frequent changes in temperature, primarily due to its inland location
330 and its lack of proximity to any large lakes. All of Missouri experiences below-freezing temperatures on a
331 yearly-basis. For example, the majority of the state typically registers, 110 days with temperatures below
332 freezing, while the Bootheel (i.e., southeast region) records, on average, 70 days of below freezing day
333 temperatures, emphasizing the typical northwest to southeast warming pattern of temperatures observed
334 in the state. Because of the large variability in temperature, the warm and cool seasons were defined from
335 an agronomic perspective, primarily taking probabilities of freezing into account. Based on the
336 climatological averages of Missouri, from 1983 to 2013, November through April registered average
337 minimum temperatures below freezing, and was considered the cool season, while May through
338 October's minimum average temperature were above freezing and constituted the warm season.

339 ~~Missouri is characterized as a continental type of climate, marked by relatively strong seasonality.~~
340 ~~Furthermore, Missouri is subject to frequent changes in temperature, primarily due to its inland location~~
341 ~~and its lack of proximity to any large lakes. All of Missouri experiences below freezing temperatures on a~~
342 ~~yearly basis. For example, the majority of the state experiences, on average, 110 days with temperatures~~
343 ~~below freezing, while the Bootheel (i.e., southeast region) registers, on average, 70 days of below~~
344 ~~freezing daytemperatures. This elaborates upon the typical northwest to southeast warming pattern of~~
345 ~~temperatures observed in the state. Because of the large variability in temperature, the warm and cool~~
346 ~~seasons were defined from an agronomic perspective, primarily taking probabilities of freezing into~~
347 ~~account. Based on the climatological averages of Missouri, from 1983 to 2013, November through April~~

348 ~~registered average minimum temperatures below freezing, and was considered the cool season, while~~
349 ~~May through October's minimum average temperature were above freezing and constituted the warm~~
350 ~~season.~~

351

352 **2.2 Rainfall data**

353 In order for the results to be comparable across the domains of the three radars it was necessary to
354 select days on which rain was observed widely across the state. Although measureable rainfall occurs on
355 more than 100 days of the year in Missouri with only 50 days typically recording greater than 25.4 mm in
356 2014 had 46 days with measurable rainfall throughout the state. Furthermore, occurrence of rain was
357 defined as the observation of an amount greater than 0.5 mm (equivalent to two rain gauge tips) in an
358 hour. This amounted to a total of approximately 300 hours of rain across those 46 days. This represents a
359 relatively standard year of rainfall for the state of Missouri. Furthermore, the days were chosen based on
360 availability of data from the National Climate Data Center's (NCDC) Hierarchal Data Storage System
361 (HDSS) for all three radars, in addition to error-free performance notes from each of the gauges used. The
362 dates analyzed were split near evenly between warm (May – October) and cool (November – April),
363 therefore encompassing an overall performance of each of the radars throughout the year with no
364 preferential bias towards rain or snow. Additionally, days were distributed evenly during the summer
365 between convective and stratiform events with a threshold of 38 dBZ (Gamache and Houze, 1982).
366 Terrestrial-based precipitation gauge data were collected from 15 separate weather stations within the
367 Missouri Mesonet, established by the Commercial Agriculture Program of University Extension (Table
368 1). All precipitation data were aggregated in hourly intervals to match the temporal resolution of the
369 gauges. Observed precipitation data were collected using Campbell Scientific TE525 tipping buckets
370 located at each of the locations for the study (Table 1). The precipitation gauges have a 15.4 cm orifice
371 which funnels to a fulcrum which registers 0.254 mm of rainfall per tip. The performance of each gauge is

372 maximized between 0 and 50°C, for which each day of the study's temperature did not exceed. Accuracy
373 in gauge measurements range between -1 to 1%, -3 to 0%, and -5 to 0% for precipitation up to 25.4 mm
374 hr⁻¹, 25.4 to 50.8 mm hr⁻¹, and 50.8 to 76.2 mm hr⁻¹, respectively, which are primarily associated with
375 local random errors and errors in tip-counting schemes (Kitchen and Blackall, 1992; Habib et al., 2001).

376 Each tipping bucket is located, approximately, 1 m above the ground in areas clear of buildings
377 and properly maintained vegetation height to mitigate turbulence effects (Habib et al., 1999). Due to the
378 well-maintained nature of the mesonet gauges, these errors were assumed negligible and, therefore,
379 allowed for the gauges to be representative of the true rainfall rate. In spite of the non-homogeneous
380 spacing of the gauges, unbiased statistics including the normalized mean bias and normalized standard
381 error were utilized.

382 In order for the results to be comparable across the domains of the three radars it was necessary to select
383 days on which rain was observed widely across the state. Although rainfall occurs on more than 100 days
384 of the year in Missouri, in 2014 only 46 days had rain widespread enough for this study. Further to this,
385 occurrence of rain was defined as the observation of an amount greater than 0.254 mm (equivalent to a
386 single rain gauge tip) in an hour. This amounted to a total of approximately 300 hours of rain across those
387 46 days. This results represents in a relatively standard year of rainfall for the state of Missouri.
388 Furthermore, the days were chosen based on availability of data from the National Climate Data Center's
389 (NCDC) Hierarchical Data Storage System (HDSS) for all three radars, in addition to error-free
390 performance notes from each of the gauges used. The dates analyzed were split near evenly between
391 warm (May–October) and cool (November–April), therefore encompassing an overall performance of
392 each of the radars throughout the year with no preferential bias towards rain or snow. Additionally, days
393 were distributed evenly during the summer between convective and stratiform events with a threshold of
394 38 dBZ (Gamache and Houze, 1982).

395 Terrestrial based (ground truthed) precipitation gauge data were collected from 15 separate weather
396 stations within the Missouri Mesonet, established by the Commercial Agriculture Program of University

Formatted: Indent: First line: 0"

Formatted: Not Highlight

397 Extension (Table 1). All precipitation data were aggregated in hourly intervals to match the temporal
398 resolution of the ground truthed gauges. Forty-six out of 365 days for the year of 2014 were analyzed
399 based on precipitation being registered across the entire study domain (Figure 1). Of these 46 days,
400 approximately 300 out of 1,104 hours of precipitation occurred such that the tipping buckets recorded
401 more than one tip (i.e., greater than 0.254 mm) for each location. This results in a relatively standard year
402 of rainfall for the state of Missouri. Furthermore, the days were chosen based on availability of data from
403 the National Climate Data Center's (NCDC) Hierarchical Data Storage System (HDSS) for all three radars,
404 in addition to error-free performance notes from each of the gauges used. The dates analyzed were split
405 near evenly between warm (May – October) and cool (November – April), therefore encompassing an
406 overall performance of each of the radars throughout the year with no preferential bias towards rain or
407 snow. Additionally, days were distributed evenly during the summer between convective and stratiform
408 events with a threshold of 38 dBZ (Camacho and Houze, 1982).

Formatted: Highlight

409 Observed precipitation data were collected using Campbell Scientific TE525 tipping buckets located at
410 each of the locations for the study (Table 1). The precipitation gauges have a 15.4 cm orifice which
411 funnels to a fulcrum which registers 0.01 mm of rainfall per tip. The performance of each gauge is
412 maximized between 0 and 50°C, for which each day of the study's temperature did not exceed. Accuracy
413 in gauge measurements range between -1 to 1%, -3 to 0%, and -5 to 0% for precipitation up to 25.4 mm
414 hr⁻¹, 25.4 to 50.8 mm hr⁻¹, and 50.8 to 76.2 mm hr⁻¹, respectively, which are, primarily, associated with
415 local random errors and errors in tip-counting schemes (Kitchen and Blackall, 1992; Habib et al., 2001).
416 Each tipping bucket is located, approximately, 1 m above the ground in areas clear of buildings and
417 properly-maintained vegetation height to mitigate turbulence effects (Habib et al., 1999). Due to the well-
418 maintained nature of the mesonet gauges, these errors were assumed negligible and, therefore, allowed for
419 the gauges to be representative of the true rainfall rate. In spite of the non-homogeneous spacing of the
420 gauges, unbiased statistics including the normalized mean bias and normalized standard error were
421 utilized.

Formatted: Highlight

422

423 **2.3 Radar data and radar rainfall algorithms**

424 Next Generation Radar (NEXRAD) level II data were retrieved from the NCDC's HDSS. Files were
425 analyzed processed using the Weather Decision Support System—Integrated Information (WDSS II)
426 program (Lakshmanan et al., 2007a) to assess reflectivity (Z) in addition to dual-polarized radar variables
427 including differential reflectivity (ZDR) and specific differential phase shift (KDP). Many different
428 quality control techniques are available (e.g., Lakshmanan et al., 2007b, 2010, 2014) and implemented
429 upon the radar data with WDSS II. Three other variables were also generated based on a KDP-based
430 smoothing field (Ryzhkov et al., 2003) for reflectivity, differential reflectivity, and specific differential
431 phase: DSMZ, DZDR, and DKDP, respectively. These were implemented to determine whether the
432 additional KDP smoothing fields tend to over- or underestimate QPE's (Simpson et al., 2016). A rain rate
433 echo classification variable (RREC) was also computed, which chooses whether an R(Z), R(KDP),
434 R(Z,ZDR), or R(ZDR, KDP) algorithm is implemented in estimating rain rates based on the radar fields
435 of Z, ZDR, and KDP (Kessinger et al., 2003) to determine whether a multi-parameter algorithm is
436 superior to a single algorithm.

437 All seven variables (Z, ZDR, KDP, DSMZ, DZDR, DKDP, and RREC) were converted from their native
438 polar grid to 256 x 256 1-km Cartesian grids, where the lowest radar elevation scans (0.5°) were used to
439 mitigate uncalculated effects from evaporation and wind drift. An average of 5-minute scans were used
440 for each of the variables, which were aggregated to hourly totals to be compared to the hourly tipping-
441 bucket accumulations. In spite of previous reports suggesting 5-minute to hourly aggregates can have
442 significant effects on QPE (e.g., Fabry et al. 1994), Shucksmith et al. (2011) present evidence that
443 accumulation overestimation did not exceed 26% for a pixel size of 1 km.

444 The latitude and longitude of each of the 15 gauges were matched with the radar pixel that corresponds to
445 the Cartesian grid value of the seven radar variables which were then implemented in rain rate

Formatted: Indent: Left: 0", First line: 0"

Formatted: Indent: First line: 0"

446 calculations. These rain rate calculations were calculated using the equations presented by Ryzhkov et al.
447 (2005) (Table 2), which were gathered from multiple studies using disdrometers to derive a relationship
448 between reflectivity, differential reflectivity, and specific differential phase (Bringi and Chandrasekar,
449 2001; Brandes et al., 2002; Illingworth and Blackman, 2002; Ryzhkov et al., 2003). Standard R(Z)
450 algorithms were also included to test whether the addition of dual polarized technology improves QPE's.
451 With the use of both Z, ZDR, KDP, and DSMZ, DZDR, and DKDP fields produced by WDSS-II, the
452 number of algorithms tested was 55. This includes the three standard single polarized algorithms
453 (stratiform, convective, and tropical) which were calculated using reflectivity R(Z), and then calculated as
454 R(DSMZ), while algorithms 1-6 (R(KDP)) were also calculated as R(DKDP). Algorithms 7-11 (R(Z,
455 ZDR)) were additionally calculated as R(Z, DZDR), R(DSMZ, ZDR), and R(DSMZ, DZDR), while the
456 same four combinations of non- and KDP smoothed fields were applied to the R(KDP, ZDR) algorithms
457 (12-15).

458

459 **2.4 Statistical analyses**

460 To test the performance of each algorithm, several statistical analyses were calculated. The average
461 difference (Bias) was calculated as

$$462 \text{Bias} = \frac{\sum (R_i - G_i)}{N} \quad (1)$$

463 where R_i is each hourly aggregated radar estimated rainfall amount calculated from one of the 55
464 algorithms, G_i is the hourly aggregated gauge (observed) measurement, and N is the total number of
465 observations which, for this study, was 1,104 hours. A second statistical parameter, the normalized mean
466 bias (NMB), was calculated as

$$467 \text{NMB} = \frac{1}{N} \frac{\sum (R_i - G_i)}{\sum G_i} \quad (2)$$

Formatted: Highlight

468 The normalized mean bias is included in the analyses due to the fact that overestimations (i.e., radar
469 estimates larger than gauge measurements) and underestimations (i.e., radar estimates smaller than gauge
470 measurements) are treated proportionately. This is directly analogous to choosing the mean absolute error
471 (MAE) opposed to the standard deviation as the MAE does not penalize smaller or larger errors,
472 obscuring the overall results (Chai and Draxler, 2014). Bias measurements (Bias and NMB) were
473 calculated to determine whether radar derived rain rates were over or under estimated in comparison to
474 the gauges. However, to calculate the overall magnitude of error associated with the performance of the
475 radars, the absolute values of (1) and (2) were performed to yield the mean absolute error (MAE), and
476 normalized standard error (NSE), respectively.

477 Several other meteorological parameters were calculated, including probability of detection
478 (PoD) which was calculated as

$$479 \text{PoD} = \frac{\sum |R_i \bullet G_i > 0 \& R_i > 0|}{\sum |G_i|} \quad (3)$$

480 where the bullet (\bullet) indicates "if", to determine how accurate the radars were at correctly detecting
481 precipitation. The probability of detection values range between 0.0 (radar did not detect any precipitation
482 correctly) and 1.0 (radar detected the occurrence of all precipitation 100% correctly). The probability of
483 false detection takes into account the amount of precipitation the radars incorrectly estimated when the
484 gauges recorded zero values, and was calculated as

$$485 \text{PoFD} = \frac{\sum R_i \bullet (G_i = 0 \& R_i > 0)}{\sum G_i} \quad (4)$$

486 Quantitative measures including the missed precipitation amount (MPA) and the false precipitation
487 amount (FPA) were defined such that

$$488 \text{MPA} = \sum R_i \bullet (G_i > 0 \& R_i = 0) \quad (5)$$

489
490
491
492
493
494
495
496
497
498
499
500
501
502
503
504
505
506
507
508
509
510

$$FPA = \sum R_i \bullet (G_i = 0 \& R_i > 0) \tag{6}$$

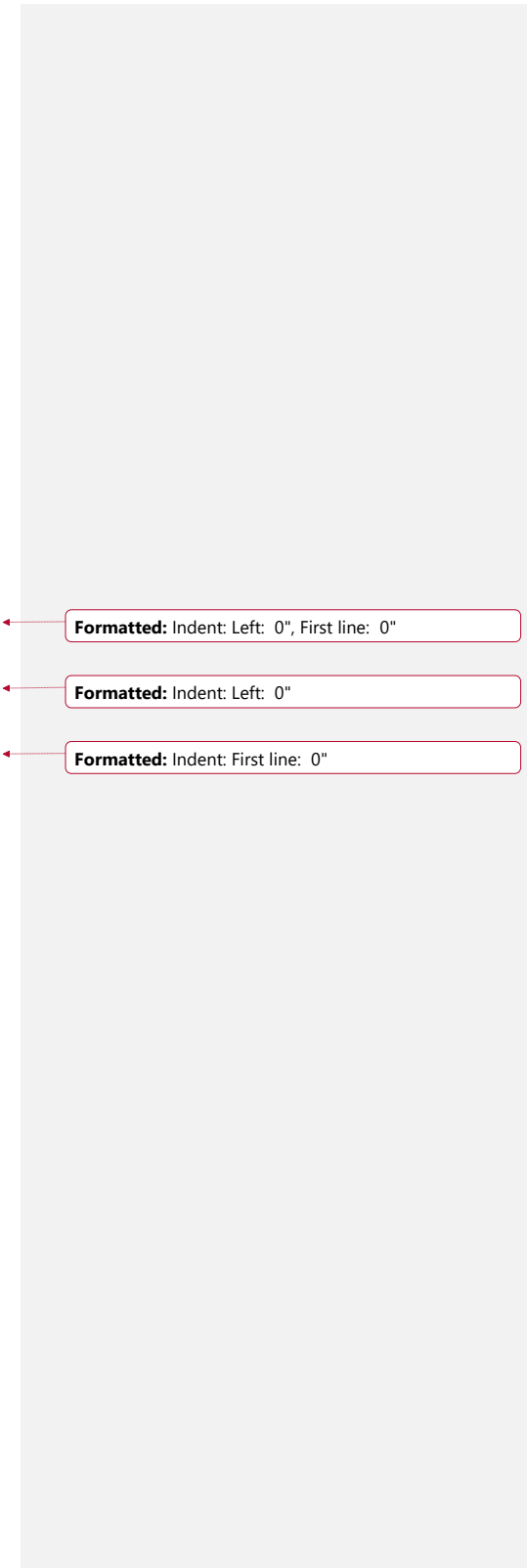
which analyzes the total amount of precipitation due to misses and false alarms. The total precipitation error was also recorded to assess the overall error from each radar.

3 Results and discussion

3.1 Overall algorithm performance

To test the overall performance of each radar, it was necessary to determine the overall best algorithm for each statistical measure. The best algorithm from each grouping of equations was determined to have the lowest normalized standard error (NSE), indicating the best performance relative to the gauge recorded precipitation amount (Ryzhkov et al., 2005). This reduces the impact of bias inherent within the dataset between warm/cool season, stratiform/convective events, and allows for statistical measurements in spite of the (typical) non-Gaussian behavior of precipitation (Kleiber et al., 2012; Alaya et al., 2017).

From the results obtained, the three R(Z) three R(DSMZ) displayed a particular bias in favor of the R(Z) Convective algorithm for all three radars with R(Z) Stratiform displaying similar performance (Figure 2a). This could be due, at least in part, to the near equal stratiform and convective precipitation regimes throughout 2014. Although errors generally increased as range increased for KEAX and KLSX, the results were nebulous for KSGF. The lowest NSE values were, typically, closest to each of the radars (between 0.4 and 0.8), with the notable exception of the closest gauge to KSGF. In general, the RREC performed worst, potentially due to the algorithm's ability to correctly assess the hydrometeors present



Formatted: Indent: Left: 0", First line: 0"
Formatted: Indent: Left: 0"
Formatted: Indent: First line: 0"

511 (Cifelli et al., 2011; Yang et al. 2016). Additionally, the poor performance by the R(DSMZ) Tropical
512 equation is due to the lack of tropical precipitation within Central Missouri. Overall, the KDP-smoothed
513 reflectivity fields (DSMZ) performed worse than their counter parts, resulting in over prediction of
514 precipitation and, thus, larger errors (Simpson et al., 2016). Errors did not exceed 2.4 for any of these
515 algorithms.

516 However, the performance of the KDP-smoothed KDP field (DKDP) performed better than the original
517 specific differential phase shift field (Figure 2b). For nearly all gauges for each of the 3 radars,
518 R(DKDP)4 performed the best, with NSE values ranging from 1.4 to 4.1. The range of NSE values were
519 largest at KEAX, while the spread was relatively small for KLSX and KSGF. In spite of this, the overall
520 spread of the performance of the 12 KDP algorithms varied greatly (average of 2 NSE units), exhibiting
521 the sensitivity of KDP estimates on QPE (Ryzhkov et al., 2005; Cunha et al., 2013). In general, the
522 NSSL-derived R(KDP) equations (i.e., equations 4-6) outperformed those from Bringi and Chandrasekar
523 (2001, equation 1), Brandes et al. (2002, equation 2), and Illingworth and Blackman (2002, equation 3).
524 Regardless, the magnitudes were all, approximately, more than 1 NSE unit than the performance of the
525 R(Z) algorithms.

526 The algorithms with the lowest NSE values were equations 7-11. For example, the overall lowest NSE
527 was at a distance of 130 km from KEAX (0.3), with no locations exceeding NSE values of 2.0 (Figure
528 2c). The large values at the closest location for KSGF (85 km, 1.3—1.9 NSE units), and the fifth closest
529 gauge to KLSX (135 km, 1.3—1.8 NSE units), Cook Station, were similar to the R(Z) and R(DSMZ)
530 results, indicating potential issues with reflectivity measurements. Additionally, these locations were the
531 closest in performance to the R(KDP) and R(DKDP) NSE values. Observations from this gauge (Cook
532 Station) indicated hail occurred during the evening of 01 August, for which KDP estimates would be
533 more ideal than Z for QPE (Ryzhkov et al. 2005; Kumjian 2013a; Cunha et al. 2015). In spite of this, the
534 overall spread in performance of the R(Z,ZDR) equations were less than the R(KDP) equations;

535 demonstrating the robust performance of $R(Z,ZDR)$ for QPE (Wang and Chandrasekar 2010; Seo et al.,
536 2015).

537 The $R(ZDR,KDP)$ algorithms performed the worst, overall (Figure 2d). In spite of the differential
538 reflectivity being implemented, the overall NSE values increased in magnitude, exceeding 6 units for the
539 second gauge analyzed by KEAX. Algorithms containing DKDP measurements performed better than
540 simply KDP, demonstrating that even with the scaling behavior of ZDR, DKDP is superior to KDP
541 estimates. This provides a potential solution to the noisy ness that tends to be exhibited in the KDP field
542 (Ruzanski and Chandrasekar 2012).

543 Due to the overall NSE values obtained, for the remainder of the analyses, equation 11 (i.e., $R(Z,ZDR)5$)
544 and equation 13 (i.e., $R(ZDR,KDP)2$) will be utilized as the best and worst algorithms, respectively.
545 Equations containing DZDR were not included in the following discussion due to the very large QPE
546 errors for each radar.

547

548 **3.2 KEAX**

549 The overall bias showed that there was a positive bias, peaking near 5.5 mm hr^{-1} at the second gauge for
550 KEAX, approximately 115 km from the radar for both the best and worst performing algorithms (Figure
551 3). This corresponds well with the spike in falsely detected precipitation recorded, which is canceled by
552 the maximum in missed precipitation at the second distance of, approximately, 150 km. The overall worst
553 algorithm, equation 13, an $R(ZDR,KDP)$ relationship, revealed a decreasing trend in bias as the distance
554 from the radar increased. For example, a bias of 4 mm hr^{-1} was observed at a distance of 75 km from the
555 radar, whereas the bias reduced to 3 mm hr^{-1} at distances near 175 km. This could be due, at least in part,
556 to the algorithm's utilization of KDP which performs poorly in frozen (especially light) precipitation
557 (Zrníc and Ryzhkov, 1996; Kumjian 2013a), causing the overestimation. Conversely, the algorithm with
558 the lowest bias was an $R(Z,ZDR)$ algorithm (equation 11). There was a maximum in the bias calculations

Formatted: Indent: Left: 0"

Formatted: Indent: First line: 0"

559 while utilizing equation 11 near 120 km, similar to equation 13, however, there was a more pronounced
560 minimum in the data near 150 km. Furthermore, it appears the data oscillates around a bias value of 0 mm
561 hr^{-1} when using equation 13. This could be due to ZDR's capability to respond to precipitation shape
562 (Kumjian 2013a), which helps to scale the reflectivity portion of the rainfall estimation algorithm to a
563 more accurate value (Seo et al., 2015). In general, the cool season displayed a larger magnitude of error in
564 terms of bias for both algorithms.

565 The normalized mean bias (NMB) reveals the same trend in values for bias but with an overall decrease in
566 magnitude. It is important to note, however, that the algorithms that tend to perform the worst (e.g.,
567 algorithms containing KDP) result in anomalous range responses which would be due, at least in part, to a
568 stronger response to precipitation type. This indicates that observations above the melting layer are
569 dominant for which QPE's tend not to be calculated (Cifelli et al., 2011; Seo et al., 2015) but are
570 important for regions devoid of adequate radar coverage (Ryzhkov et al., 2003; Simpson et al., 2016).

571 The absolute bias and normalized standard error (NSE) shows the same maxima in the data at the second
572 gauge (Brunswick) that was present in the bias data (6.2 mm hr^{-1} and 5.6, respectively). However, a
573 second maxima is located at the fifth gauge at, approximately, 150 km (Linneus) with values of 5.9 mm
574 hr^{-1} and 4.0, respectively. Bright band issues are detected due, at least in part, to the increased missed
575 precipitation amount (240 mm) at this particular distance for the R(ZDR,KDP) equation (i.e., worst
576 performing algorithm). There was also a pronounced minimum in the absolute bias and NSE results at the
577 fourth gauge for equations 11 and 13, 4.0 mm hr^{-1} and 0.8 mm hr^{-1} , and 2.8 and 0.8, respectively,
578 potentially indicating an idealized range of QPE for KEAX. Furthermore, the historical records at this
579 particular gauge showed less issues (e.g., clogging) than any of the others analyzed by the KEAX radar.
580 This highlights the importance of choosing ground truth data, in particular tipping buckets which are
581 prone to numerous errors (Ciach and Krajewski, 1999b). The largest contributions to the NSE and NMB
582 were due to the warm season.

583 The probability of detection (PoD) results indicate a large difference in algorithm choice for correctly
584 detecting precipitation. The low PoD at approximately 150 km, indicates overshooting of the beam. This
585 is further evidenced by the MPA results, as about 225 mm of precipitation was missed by the radar at 150
586 km, whereas only 100 mm of precipitation was missed by the radar at the second gauge at 120 km.
587 Although equation 11, an $R(Z,ZDR)$ algorithm was superior in terms of the bias, the same algorithm with
588 a KDP smoothed reflectivity value, $R(DSMZ,ZDR)$ revealed the overall least amount of falsely missed
589 precipitation (by 10 mm). However, the summation of the amount of precipitation falsely detected (PoFD)
590 by KEAX showed a larger source of error than the MPA in terms of magnitude. For example, at the
591 second (fifth) gauge, only 100 (225) mm of precipitation was missed by the radar, but over 700 (725) mm
592 of precipitation was incorrectly estimated by the radar.

593 Correlation coefficient (CC) values for any of the 9 stations analyzed by KEAX ranges from 0.02
594 (Linneus, 151 km) to 0.93 for the cool season (St. Joseph, 115 km). The lowest R^2 were due to a
595 combination of false alarms and misses. For example, the CC for the warm seasons at Sanborn (170 km)
596 and Jefferson Farm (173 km) were 0.22 and 0.24, respectively, whereas when the instances of false
597 alarms and misses were removed, increased to 0.48 and 0.52. Few locations (Brunswick, 114 km and
598 Versailles, 129 km) saw little improvement in the CC values when only hits were analyzed (less than 0.1
599 increase), indicating the mean absolute error (in terms of hits) contributed the largest portion of error.

600

601 **3.3 KLSX**

602 Unlike the KEAX data, the gauges used for analyses for the KLSX radar span between 90—150 km.
603 Furthermore, 5 out of the 8 gauges were located within 10 km of range from one another, near 140 km
604 from the radar, limiting the data available for analyses between 100 and 140 km (Figure 5).

605 The bias and NMB both show a relatively modest peak in values near the second gauge of 5 mm, which
606 decreases to approximately 3.6 mm at the third gauge, 120 km from the radar. The worst performing

Formatted: Indent: Left: 0"

Formatted: Indent: First line: 0"

607 algorithm, equation 13, was the same $R(ZDR, KDP)$ relation as the worst KEAX bias and NMB data.
608 Additionally, the overall trend of decreasing bias and NMB as distance from the radar increases was
609 noted, presumably due to overshooting effects similar to the KEAX data. Furthermore, the overall non-
610 biased results from the $R(Z, ZDR)$ equation demonstrates its robust capabilities in QPE, in spite of its
611 sensitivity to calibration (Zrníc et al., 2005; Bechini et al., 2008).

612 The double maxima in the absolute bias graph are present as with the KEAX data, but are not as
613 pronounced. For example, the absolute bias at 95 km and 140 km from KLSX were 5.9 mm and 1.1 mm,
614 and 4.9 mm and 1.4 mm for equations 13 and 11, respectively. Additionally, the overall minima in the
615 absolute bias for both KEAX and KLSX are at, approximately, 125 km from the radar (3.9 mm hr^{-1} and
616 1.0 mm hr^{-1} , respectively, for equations 13 and 11). The relative distance from the radars are the same,
617 where the two maxima for KEAX were at 115 and 150 km, while the maxima were at, approximately,
618 100 and 140 km for KLSX. The overall best and worst performing algorithms at KLSX for the absolute
619 bias and NSE were equations 11 and 13, the $R(Z, ZDR)$ and $R(ZDR, KDP)$ algorithms, respectively.

620 The magnitude of error in terms of absolute bias, normalized mean bias, and normalized standard error,
621 all showed a decreasing pattern as distance from KLSX increased. This was due, primarily, from a
622 maximum in the false precipitation amount at 95 km from the radar. Historical notes at this location
623 indicate frequent clogging of the rain gauge, either due to bugs or leaves. From a particular series of
624 events spanning from 01 to 04 April and 01 to 03 August, 2014, over 130 mm of precipitation occurred
625 during each period which was not captured by the gauge, resulting in a large amount of overall error.
626 These results indicate the important of dual gauges in the same vicinity (Krajewski et al. 1998; Ciach and
627 Krajewski 1999). Interestingly, the cool season displayed a larger NSE (5 % for $R(ZDR, KDP)$)
628 potentially due to the very low probability of detection (0.2) at this range of 118 km.

629 One of the main differences between the KLSX and KEAX data was the decreased probability of
630 detection at 120 km for KLSX, while there was an increased probability of detection for KEAX. In
631 general, the PoD values were worse for KLSX when compared to KEAX. For example, equation 11 had

632 no PoD values below 0.90, whereas no PoD values exceeded 0.84 for KLSX. There was also a slight
633 trend of increasing PoD values as distance from the St. Louis radar increased and, at one point near 140
634 km, the best algorithm, R(DSMZ) convective and the worst algorithm, KDPI, were not significantly
635 different ($p < 0.10$). Additionally, the maxima in the PoD while utilizing KDPI corresponds to a minima
636 in the R(DSMZ) detection percentage, which is well correlated by the similarly valued MPA results.
637 The missed precipitation amount (MPA) displayed the cool season contributed the most, whereas the
638 warm season contributed the most amount of false precipitation amount. The R(Z,ZDR) equation only
639 registered, on average, 25 mm of MPA and 160 mm of FPA, whereas the R(ZDR,KDP) equation was
640 very dependent upon range. For example, the FPA from R(ZDR,KDP) decreased as range increased from
641 the radar from a maximum of, approximately, 850 mm to 620 mm. However, the fifth furthest gauge (137
642 km from KLSX) displayed a sharp increase in the MPA for both cool seasons (above 100 mm).

643

644

645 ——— 3.4 KSGF

646 ———

647 In spite that the KLSX and KEAX data strongly suggests false precipitation errors near 100 km in
648 addition to bright banding near 150 km from the radars, the KSGF results reveal an overall smooth
649 decrease (increase) of error with range (Figure 7) for R(ZDR,KDP) and R(Z,ZDR), accordingly. One of
650 the main reasons for this could be due to the fact that only 5 gauges were analyzed from KSGF (the
651 fewest of the 3 radars analyzed), smoothing the overall trend lines.

652 The bias remained relatively constant near -0.3 mm for R(Z,ZDR), whereas the bias exhibited a sharp
653 decrease from 4 mm to 2.7 mm over a distance of, approximately, 100 km. In general, the cool season

Formatted: Indent: First line: 0"

654 displayed the lower of bias magnitudes when compared to the warm season, similar to the KEAX results.
655 This may be due, at least in part, to the low PoFD values for the warm season close to the KSGF radar.
656 Similar to the bias, the absolute bias for R(Z,ZDR) was constant at all ranges (near 1 mm) whereas the
657 R(ZDR,KDP) equation decreased from 5.2 mm to 3.8 mm. This is potentially due to the low cool season
658 PoD values (below 0.6), while the warm season R(ZDR,KDP) values (near 0.8) remained constant. A
659 larger contribution from more correctly detected precipitation in addition to the decreasing trends in the
660 NMB and NSE would result in a lower absolute bias.

661 The closest location (90 km) typically displayed the largest errors for the R(ZDR,KDP) equation, and
662 then decreased in error magnitude as range increased. In spite of this, the PoFD results indicate both
663 algorithms increased in PoFD values as range increased, with the warm season typically dominating,
664 particularly due to the large convective clouds dominate in the warm season. False detection values as
665 low as 0.01 for the cool season while utilizing R(Z,ZDR) were observed at distances near 100 km and 140
666 km from the radar.

667 Normalized standard error values increased from 0.7 % at a distance of 105 km to 1.8 % at a distance of
668 185 km for R(Z,ZDR). Large NSE values for the warm season (7.5 %) were calculated for R(ZDR,KDP)
669 which decreased to 3.8 % at 185 km from the radar. Furthermore, this was the only instance when the
670 warm season was less than the cool season in terms of NSE. Otherwise, the overall NSE decreased from 5
671 % to 3.9 % for R(ZDR,KDP). The NMB followed a similar trend for the KDP containing algorithm, with
672 a noticeable exception at the second gauge (105 km from KSGF), where the overall NSE was closer to the
673 warm than cool season. This is due to the low PoFD values at this location, in addition to a smaller
674 difference between the two algorithm's FPA measurements.

675 The MPA results, unlike for KEAX and KLSX, displayed a larger range of performance between seasons.
676 However, the warm season still exhibited the overall best performance in terms of MPA, yet contributed
677 the most to the FPA for both R(Z,ZDR) and R(ZDR,KDP). In spite of the MPA typically increasing as

678 range increased, the FPA was more nebulous. For example, the second gauge (105 km from KSGF) had
679 the overall lowest NSE (0.8 %), MPA (15 mm), and FPA (95 mm) for R(Z,ZDR). The third-furthest
680 location (142 km) resulted in slightly larger errors, overall, while the fourth-furthest location had errors
681 similar to the second gauge (105 km). Then, at the furthest tipping bucket location (185 km), NSE values
682 increased, whereas FPA and MPA decreased. Therefore, the furthest location's errors are due, primarily,
683 from discrepancies between precipitation magnitude between the gauge and radar.

684 Excluding Versailles (142 km from KSGF), the cool season exhibited larger R^2 values in comparison to
685 the cool season (Figure 8). Furthermore, CC values exceeded 0.9 when false alarms and misses were
686 excluded from Mt. Grove (101 km) and was 0.84 when included. Otherwise, the other four stations
687 analyzed by the Springfield radar displayed many counts of false alarms and misses, leading to low R^2
688 values.

689 ——— Due to the relatively large ranges from the Springfield (KSGF) radar, most of the correlation
690 coefficient values were low in comparison to either KLSX or KEAX. For the warm (cool) season without
691 false alarms and misses, R^2 values ranged from 0.44 (0.38) and 0.34 (0.36) for KLSX and KSGF,
692 respectively, at Cook Station (119 and 185 km). Similarly, the CC values ranged from 0.61 (0.71) to 0.42
693 (0.56) at Green Ridge (76 and 154 km) for KEAX and KSGF, accordingly.

694

Formatted: Indent: First line: 0"

695

696

697 **4 ——— Conclusions**

Formatted: Indent: Left: 0", First line: 0"

698 Dual polarization technology was implemented to the National Weather Service Next Generation Radar
699 network in the Spring of 2012 to, primarily, improve quantitative precipitation estimation and
700 hydrometeor classification. The current study observed over 1,100 hours of precipitation data with three

Formatted: Indent: First line: 0"

701 separate radars in Missouri using 55 algorithms including the three conventional R(Z) radar rain rate
702 estimation algorithms (stratiform, convective, and tropical) along with a myriad of R(KDP), R(Z,ZDR),
703 and R(ZDR,KDP) algorithms which can be found in Ryzhkov et al. (2005). Additionally, a KDP-
704 smoothing field of reflectivity, differential reflectivity, and the specific differential phase shift (DSMZ,
705 DZDR, and DKDP, respectively) were measured and used for analyses. Unlike previous studies, the
706 current work emphasizes the amount of precipitation correctly and incorrectly estimated by the radar in
707 comparison to the terrestrial based precipitation gauges through measurements of the missed and false
708 precipitation amount.

709 For all three radars, Kansas City, St. Louis, and Springfield, MO (KEAX, KLSX, and KSGF,
710 respectively), the majority of precipitation error (over 60%) was contributed by the amount of
711 precipitation falsely detection by the radar (up to 725 mm), while 20% was due to the radar missing the
712 precipitation (up to 225 mm) for KEAX. Similar magnitudes of error were reported for KLSX and KSGF,
713 with an overall error in precipitation for each radar ranging between 250 mm for the best performing of
714 the 55 algorithms, equation 11 (an R(Z,ZDR) algorithm), and up to 2000 mm for the worst performing
715 algorithms, R(ZDR,KDP) equation 13. The R(Z,ZDR) equation (an NSSL algorithm) was determined to
716 be the most robust due to it registering the lowest NSE.

717 The data was divided into summer (May—October) and winter (November—April) months resulting in
718 652 hours for summer, and 452 hours for winter (59 and 41% of the entire data, respectively). Despite the
719 winter data contributing less than the summertime data, it accounted for 20% of the overall MPA, and
720 40% to the overall PoFD. The R^2 values were less during the winter in comparison to the warm season
721 primarily due to the smaller magnitude of precipitation that occurred. Furthermore, CC values increased
722 by as much as 0.4 when instances of hits and misses were removed from the analyses, resulting in the
723 warm season to outperform the cool season CC values at particularly short ranges from the radar.

724 These results aid in our understanding in the possibilities for hydrometeorological studies. Nearly 50% of
725 the 1,100 hours analyzed for the study consisted of either falsely estimated precipitation by the radar, or

726 missed by the radar. Furthermore, these errors accumulate between 500 to 2,000 mm of precipitation
727 depending on the algorithms chosen. Although the overall performance increased when false alarms and
728 misses were removed, correlation coefficient values still, typically, remained below 0.50 at ranges beyond
729 130 km.

730 Furthermore, results demonstrate the issues with analyzing QPE from a single gauge, explaining why the
731 Community Collaborative Rain, Hail, and Snow Network (Kelsch 1998; Cifelli et al., 2005; Reges et al.,
732 2016) tends to be more utilized since results have shown that measurements or quality-controlled
733 techniques made by CoCoRaHS are significantly more accurate than rain gauges (Simpson et al., 2017),
734 especially for convective events (Moon et al. 2009).

735

736 **Author Contribution.** N. Fox designed the experiment and provided feedback while M. Simpson carried
737 out the calculations and wrote the manuscript.

738 **Acknowledgements.** This material is based upon work supported by the National Science Foundation
739 under Award Number IIA-1355406. Any opinions, findings, and conclusions or recommendations
740 expressed in this material are those of the authors and do not necessarily reflect the views of the National
741 Science Foundation.

742

743 **References**

744 Alaya, M.A., Ourda, T.B.M.J., Chebana, F.: Non-Gaussian spatiotemporal simulation of multisite
745 precipitation: Downscaling framework. *Climate Dynamics*, 2017. doi: [https://doi.org/10.1007/s00382-](https://doi.org/10.1007/s00382-017-3578-0)
746 [017-3578-0](https://doi.org/10.1007/s00382-017-3578-0).

747 Anagnostou, M.N., Anagnostou, E.N., Vulpiani, G., Montopoli, M., Marzano, F.S., Vivekanandan, J.:
748 Evaluation of X-band polarimetric radar estimates of drop-size distributions from coincident S-band

Formatted: Indent: Left: 0"

Formatted: Indent: Left: 0", First line: 0"

749 polarimetric estimated and measured raindrop spectra. *IEEE Transactions on Geoscience and Remote*
750 *Sensing*, 46, 3067–3075, 2008.

751 Bechini, R., Baldini, L., Cremonini, R., Gorgucci, E.: Differential reflectivity calibration for operational
752 radars. *Journal of Atmospheric and Oceanic Technology*, 25, 1542–1555, 2009.

753 Berne, A. and Uijlenhoet, R.: A stochastic model of range profiles of raindrop size distributions:
754 application to radar attenuation correction, *Geophysical Research Letters*, 32, 2005, doi:
755 <https://doi.org/10.1029/2004GL021899>.

756 Berne, A. and Krajewski, W.F.: Radar for hydrology: Unfulfilled promise or unrecognized potential?
757 *Advances in Water Resources*, 51, 357–366, 2013.

758 Bringi, V.N. and Chandrasekar, V.: Polarimetric Doppler weather radar, principles and applications.
759 Cambridge University Press: Cambridge, UK, 636, 2001.

760 Brandes, E.A., Zhang, G., Vivekanandan, J.: Experiments in rainfall estimation with a polarimetric radar in
761 a subtropical environment, *Journal of Applied Meteorology*, 41, 674–685, 2002.

762 Brandes, E.A., Zhang, G., Vivekanandan, J.: Drop size distribution retrieval with polarimetric radar: model
763 and application, *Journal of Applied Meteorology*, 43, 461–475, 2004.

764 Chai, T., Draxler, R.R.: Root mean square error (RMSE) or mean absolute error (MAE)? — Arguments
765 against avoiding RMSE in the literature, *Geoscientific Model Development*, 7, 1247–1250, 2014.

766 Ciach, G.J., Krajewski, W.F.: On the estimation of radar rainfall error variance. *Advances in Water*
767 *Resources*, 22, 585–595, 1999a.

768 Ciach, G.J. and Krajewski, W.F.: Radar rain gauge comparisons under observational uncertainties. *Journal*
769 *of Applied Meteorology*, 38, 1519–1525, 1999b.

770 Giach, G.J.: Local random errors in tipping bucket rain gauge measurements. *Journal of Atmospheric and*
771 *Oceanic Technology*, 20, 752-759, 2002.

772 Gifelli, R., Doesken, N., Kennedy, P., Carey, L.S., Rutledge, S.A., Gimmestad, C., Depue, T.: The community
773 collaborative rain, hail, and snow network: Informal education for scientists and citizens. *Bulletin of the*
774 *American Meteorological Society*, 86, 1069-1077, 2005.

775 Cunha, L.K., Smith, J.A., Baeck, M.L., Krajewski, W.F.: An early performance of the NEXRAD dual-
776 polarization radar rainfall estimates for urban flood applications. *Weather and Forecasting*, 28, 1478-
777 1497, 2013.

778 Cunha, L.K., Smith, J.A., Krajewski, W.F., Baeck, M.L., Seo, B.: NEXRAD NWS polarimetric precipitation
779 product evaluation for IFloods. *Journal of Hydrometeorology*, 16, 1676-1699, 2015.

780 Delrieu, G., Andrieu, H., Creutin, J.D.: Quantification of path-integrated attenuation for X- and C-band
781 weather radar systems operating in Mediterranean heavy rainfall. *Journal of Applied Meteorology*, 39,
782 840-850, 2000.

783 Fabry, F., Bellon, A., Duncan, M.R., Austin, G.L.: High resolution rainfall measurements by radar for very
784 small basins: the sampling problem reexamined. *Journal of Hydrology*, 161, 415-428, 1994.

785 Fairman, J.G., Schultz, D.M., Kirschbaum, D.J., Gray, S.L., Barrett, A.I.: A radar-based rainfall climatology
786 of Great Britain and Ireland. *Weather*, 70, 153-158, 2012. doi: <https://doi.org/10.1002/wea.2486>.

787 Gamache, J.F. and Houze, R.A.: Mesoscale air motions associated with a tropical squall line. *Monthly*
788 *Weather Review*, 110, 118-135, 1982.

789 Giangrande, S.E. and Ryzhkov, A.V.: Estimation of rainfall based on the results of polarimetric echo
790 classification. *Journal of Applied Meteorology*, 47, 2445-2460, 2008.

791 Gorgucci, E., Scarchilli, G., Chandrasekar, V.: Calibration of radars using polarimetric techniques. IEEE
792 Transactions in Geoscience and Remote Sensing, 30, 853–858, 1992. Gorgucci, E., Scarschilli, G.,
793 Chandrasekar, V., Bringi, V.N.: Measurement of mean raindrop shape from polarimetric radar
794 observations. Journal of the Atmospheric Sciences, 57, 3406–3413, 2000.

795 Gorgucci, E., Baldini, L., Chandrasekar, V.: What is the shape of a raindrop? An answer from radar
796 measurements. Journal of the Atmospheric Sciences, 63, 3033–3044, 2006.

797 Goudenhoofdt, E., Delobbe, L.: Long-term evaluation of radar QPE using VPR correction and radar-gauge
798 merging. International Association of Hydrological Sciences Publications, 351, 249–254, 2012.

799 Goudenhoofdt, E., Delobbe, L.: Generation and verification of rainfall estimates from 10-yr volumetric
800 weather radar measurements. Journal of Hydrometeorology, 13, 1191–1204, 2016.

801 Gourley, J.J., Giangrande, S.E., Hong, Y., Flamig, Z., Schuur, T., Vrugt, J.: Impacts of polarimetric radar
802 observations on hydrologic simulation. Journal of Hydrometeorology, 11, 781–796, 2010.

803 Habib, E., Krajewski, W.F., Nespor, V., Kruger, A.: Numerical simulation studies of rain-gauge data
804 correction due to wind effect. Journal of Geophysical Research, 104, 723–734, 1999.

805 Habib, E., Krajewski, W.F., Kruger, A.: Sampling errors of tipping-bucket rain-gauge measurements.
806 Journal of Hydrological Engineering, 6, 159–166, 2001.

807 Haylock, M.R., Hofstra, N., Klein Tank, A.M.G., Klok, E.J., Jones, P.D., New, M.: A European daily high-
808 resolution gridded data set of surface temperature and precipitation for 1950–2006. Journal of
809 Geophysical Research, 113, 2008. doi: <https://doi.org/10.1029/2008JD010201>

810 Holleman, I., Huuskonen, A., Gill, R., Tabary, P.: Operational monitoring of radar differential reflectivity
811 using the sun. Journal of Atmospheric and Oceanic Technology, 27, 881–887, 2010.

812 Hubbert, J.C.: Differential reflectivity calibration and antenna temperature. *Journal of Atmospheric and*
813 *Oceanic Technology*, 34, 1885–1906, 2017.

814 Illingworth, A., Blackman, T.A.: The need to represent raindrop size spectra as normalized gamma
815 distributions for the interpretation of polarization radar observations. *Journal of Applied Meteorology*,
816 41, 286–297, 2002.

817 Kelsch, M.: The Fort Collins flash flood: Exceptional rainfall and urban runoff. Preprints, 19th Conference
818 on severe local storms, Minneapolis, MN, American Meteorological Society, 404–407, 1998.

819 Kitchen, M. and Blackall, M.: Representativeness errors in comparisons between radar and gauge
820 measurements of rainfall. *Journal of Hydrology*, 134, 13–33, 1992.

821 Kleiber, W., Katz, R.W., Rajagopalan, B.: Daily spatiotemporal precipitation simulation using latent and
822 transformed Gaussian processes. *Water Resources Research*, 48, 2012. doi:
823 <https://doi.org/10.1029/2011WR011105>. Kessinger, C., Ellis, S., Van Andel, J.: The radar echo classifier: a
824 fuzzy logic algorithm for the WSR-88D. 19th Conf. on Inter. Inf. Proc. Sys. (IIPS) for Meteor., Ocean., and
825 Hydr., Amer. Meteor. Soc., Long Beach, CA, 2003.

826 Kitchen, M. and Jackson, P.M.: Weather radar performance at long range – simulated and observed.
827 *Journal of Applied Meteorology*, 32, 975–985, 1993.

828 Krajewski, W.F., Kruger, A., Nespor, V.: Experimental and numerical studies of small-scale rainfall
829 measurements and variability. *Water Science and Technology*, 37, 131–138.

830 Kumjian, M.R.: Principles and applications of dual-polarization weather radar. Part 1: Description of the
831 polarimetric radar variables. *Journal of Operational Meteorology*, 1, 226–242, 2013a.

832 Kumjian, M.R.: Principles and applications of dual-polarization weather radar. Part 2: Warm and cold
833 season applications. *Journal of Operational Meteorology*, 1, 243–264, 2013b.

834 Kumjian, M.R.: Principles and applications of dual-polarization weather radar. Part 3: Artifacts. *Journal of*
835 *Operational Meteorology*, 1, 265–274, 2013c.

836 Lakshmanan, V., Smith, T., Stumpf, G., Hondl, K.: The warning decision support system—integrated
837 information. *Weather and Forecasting*, 22, 596–612, 2007a.

838 Lakshmanan, V., Fritz, A., Smith, T., Hondl, K., Stumpf, G.: An automated technique to quality control
839 radar reflectivity data. *Journal of Applied Meteorology and Climatology*, 46, 288–305, 2007b.

840 Lakshmanan, V., Zhang, J., Howard, K.: A technique to censor biological echoes in radar reflectivity data.
841 *Journal of Applied Meteorology and Climatology*, 49, 453–462, 2010.

842 Lakshmanan, V., Karstens, C., Krause, J., Tang, L.: Quality control of weather radar data using
843 polarimetric variables. *Journal of Atmospheric and Oceanic Technology*, 31, 1234–1249, 2014.

844 Moon, J.T., Guinan, P.E., Snider, D.J., Lupo, A.R.: CoCoRaHS in Missouri: Four years later, the importance
845 of observations. *Transactions of the Missouri Academy of Science*, 43, 7–18, 2009.

846 Park, H.S., Ryzhkov, A.V., Zrnich, D.S.: The hydrometeor classification algorithm for the polarimetric WSR-
847 88DL: Description and application to an MCS. *Weather and Forecasting*, 24, 730–748, 2009.

848 Reges, H.W., Doesken, N., Turner, J., Newman, N., Bergantino, A., Schwalbe, Z.: CoCoRaHS: The
849 evolution and accomplishments of a volunteer rain-gauge network. *Bulletin of the American*
850 *Meteorological Society*, 97, 1831–1846, 2016.

851 Ruzanski, E., Chandrasekar, V.: Nowcasting rainfall fields derived from specific differential phase. *Journal*
852 *of Applied Meteorology and Climatology*, 51, 1950–1959, 2012.

853 Ryzhkov, A.V., Giangrande, S., Schurr, T.: Rainfall measurements with the polarimetric WSR-88D radar.
854 *National Severe Storms Laboratory Rep. Norman: OK*, 98, 2003.

855 Ryzhkov, A.V., Giangrande, S., Schurr, T.: Rainfall estimation with a polarimetric prototype of WSR-88D.
856 *Journal of Applied Meteorology*, 44, 502–515, 2005.

857 Scarchilli, G., Gorgucci, E., Chandrasekar, V., Dobaie, A.: Self-consistency of polarization diversity
858 measurement of rainfall. *IEEE Transactions in Geoscience and Remote Sensing*, 34, 22–26, 1996.

859 Shucksmith, P.E., Sutherland-Stacey, L., Austin, G.L.: The spatial and temporal sampling errors inherent
860 in low resolution radar estimates of rainfall. *Meteorological Applications*, 18, 354–360, 2011.

861 Simpson, M.J., Hubbard, J.A., Fox, N.I.: Ground truthed performance of single and dual polarized radar
862 rain rates at large ranges. *Hydrological Processes*, 30, 3692–3703, 2016.

863 Simpson, M.J., Hirsch, A., Grempler, K., Lupo, A.R.: The importance of choosing precipitation datasets.
864 *Hydrological Processes*, 1–13. doi: <https://doi.org/10.1002/hyp.11381>.

865 Seo, B.-C., Dolan, B., Krajewski, W., Rutledge, S.A., Petersen, W.: Comparison of single and dual
866 polarization based rainfall estimates using NEXRAD data for the NASA Iowa Flood Studies project.
867 *Journal of Hydrometeorology*, 16, 1658–1675, 2015.

868 Smith, J.A., Seo, D.J., Baeck, M.L., Hudlow, M.D.: An intercomparison study of NEXRAD precipitation
869 estimates. *Water Resources Research*, 32, 2035–2045, 1996.

870 Straka, J.M., Zrnich, D.S., Ryzhkov, A.V.: Bulk hydrometeor classification and quantification using
871 polarimetric radar data: Synthesis of relations. *Journal of Applied Meteorology*, 39, 1341–1372, 2000.

872 Yang, L., Yang, Y., Liu, P., Wang, L.: Radar derived quantitative precipitation estimation based on
873 precipitation classification. *Advances in Meteorology*, 2016, 2016. doi:
874 <https://doi.org/10.1155/2016/2457489>.

875 Zhang, G., Vivekanandan, J., Brandes, E.A.: A method for estimating rain rate and drop size distribution
876 from polarimetric radar measurements. *IEEE Transactions on Geoscience and Remote Sensing*, 39, 830–
877 841, 2001.

878 ~~Zrníc, D.S., Ryzhkov, A.V.: Advantages of rain measurements using specific differential phase. Journal of~~
879 ~~Atmosphere and Oceanic Technology, 13, 454–464, 1996.~~
880 ~~Zrníc, D.S., Ryzhkov, A.V.: Polarimetry for weather surveillance radars. Bulletin of American~~
881 ~~Meteorological Society, 80, 389–406, 1999.~~
882 ~~Zrníc, D.S., Melnikov, V.M., Carter, J.K.: Calibrating differential reflectivity on the WSR-88D. Journal of~~
883 ~~Atmospheric and Oceanic Technology, 23, 944–951, 2005.~~

884

Formatted: Indent: First line: 0"

885 **2.3 Radar data and radar-rainfall algorithms**

886 Next Generation Radar (NEXRAD) level-II data were retrieved from the NCDC’s HDSS. Files
887 were processed using the Weather Decision Support System – Integrated Information (WDSS-II) program
888 (Lakshmanan et al., 2007a) to assess reflectivity (Z) in addition to dual-polarized radar variables
889 including differential reflectivity (ZDR) and specific differential phase shift (KDP). Three other variables
890 were also generated based on a KDP-based smoothing field (Ryzhkov et al., 2003) for reflectivity,
891 differential reflectivity, and specific differential phase: DSMZ, DZDR, and DKDP, respectively. These
892 were implemented to determine whether the additional KDP-smoothing fields tend to over- or
893 underestimate QPE’s (Simpson et al., 2016). A rain rate echo classification variable (RREC) was also
894 computed, which chooses whether an R(Z), R(KDP), R(Z,ZDR), or R(ZDR, KDP) algorithm is
895 implemented in estimating rain rates based on the radar fields of Z, ZDR, and KDP (Kessinger et al.,
896 2003) to determine whether a multi-parameter algorithm is superior to a single algorithm.

897 All seven variables (Z, ZDR, KDP, DSMZ, DZDR, DKDP, and RREC) were converted from
898 their native polar grid to 256 x 256 1 km Cartesian grids, where the lowest radar elevation scans (0.5°)
899 were used to mitigate uncalculated effects from evaporation and wind drift. An average of 5 minute scans
900 were used for each of the variables, which were aggregated to hourly totals to be compared to the hourly
901 tipping-bucket accumulations. In spite of previous reports suggesting 5 minute to hourly aggregates can

902 have significant effects on QPE (e.g., Fabry et al. 1994), Shucksmith et al.'s (2011) criterion of present
903 accumulation exceeding 26% for a pixel size of 1 km was not reached.

904 The latitude and longitude of each of the 15 gauges were matched with the radar pixel that
905 corresponds to the Cartesian grid value of the seven radar variables which were then implemented in rain
906 rate calculations. These rain-rate calculations were calculated using the equations presented by Ryzhkov
907 et al. (2005) (Table 2), which were gathered from multiple studies using disdrometers to derive a
908 relationship between reflectivity, differential reflectivity, and specific differential phase (Bringi and
909 Chandrasekar, 2001; Brandes et al., 2002; Illingworth and Blackman, 2002; Ryzhkov et al., 2003).
910 Standard R(Z) algorithms were also included to test whether the addition of dual-polarized technology
911 improves QPE's.

912 With the use of both Z, ZDR, KDP, and DSMZ, DZDR, and DKDP fields produced by WDSS-II,
913 the number of algorithms tested was 55. This includes the three standard single-polarized algorithms
914 (stratiform, convective, and tropical) which were calculated using reflectivity R(Z), and then calculated as
915 R(DSMZ), while algorithms 1-6 (R(KDP)) were also calculated as R(DKDP). Algorithms 7-11 (R(Z,
916 ZDR)) were additionally calculated as R(Z, DZDR), R(DSMZ, ZDR), and R(DSMZ, DZDR), while the
917 same four combinations of non- and KDP-smoothed fields were applied to the R(KDP, ZDR) algorithms
918 (12-15). Quality controlling methods for the algorithms include mitigation of clutter, sun spikes, beam
919 blockage, anomalous propagation, and removal of non-precipitation echoes (including biological and
920 chaff returns) through w2qcnn the w2qcndp algorithms (Lakshmanan et al., 2007b, 2010, 2014).

921

922 2.4 Statistical analyses

923 To test the performance of each algorithm, several statistical analyses were calculated. The
924 average difference (Bias) was calculated as

Formatted: Indent: First line: 0.5"

925
$$Bias = \frac{\sum (R_i - G_i)}{N} \quad (1)$$

926 where R_i is each hourly aggregated radar estimated rainfall amount calculated from one of the 55
927 algorithms, G_i is the hourly aggregated gauge (observed) measurement, and N is the total number of
928 observations which, for this study, was 300 hours. A second statistical parameter, the normalized mean
929 bias (NMB), was calculated as

930
$$NMB = \frac{1}{N} \frac{\sum (R_i - G_i)}{\sum G_i} \quad (2)$$

931 The normalized mean bias is included in the analyses due to the fact that overestimations (i.e., radar
932 estimates larger than gauge measurements) and underestimations (i.e., radar estimates smaller than gauge
933 measurements) are treated proportionately. This is directly analogous to choosing the mean absolute error
934 (MAE) opposed to the standard deviation as the MAE does not penalize smaller or larger errors,
935 obscuring the overall results (Chai and Draxler, 2014). Bias measurements (Bias and NMB) were
936 calculated to determine whether radar derived rain rates were over- or under-estimated in comparison to
937 the gauges. However, to calculate the overall magnitude of error associated with the performance of the
938 radars, the absolute values of (1) and (2) were performed to yield the mean absolute error (MAE), and
939 normalized standard error (NSE), respectively.

940 Several other meteorological parameters were calculated, including probability of detection
941 (PoD) which was calculated as

942
$$PoD = \frac{\sum |R_i \bullet G_i > 0 \ \& \ R_i > 0|}{\sum |G_i|} \quad (3)$$

943 where the bullet (\bullet) indicates "if", to determine how accurate the radars were at correctly detecting
944 precipitation. The probability of detection values range between 0.0 (radar did not detect any precipitation

Field Code Changed

Field Code Changed

Field Code Changed

Field Code Changed

945 correctly) and 1.0 (radar detected the occurrence of all precipitation 100% correctly). The probability of
946 false detection takes into account the amount of precipitation the radars incorrectly estimated when the
947 gauges recorded zero values, and was calculated as

$$948 \quad PoFD = \frac{\sum R_i \cdot (G_i = 0 \& R_i > 0)}{\sum G_i} \quad (4)$$

Field Code Changed

949 Quantitative measures including the missed precipitation amount (MPA) and the false precipitation
950 amount (FPA) were defined such that

$$951 \quad MPA = \sum R_i \cdot (G_i > 0 \& R_i = 0) \quad (5)$$

Field Code Changed

$$952 \quad FPA = \sum R_i \cdot (G_i = 0 \& R_i > 0) \quad (6)$$

Field Code Changed

953 which analyzes the total amount of precipitation due to misses and false alarms. The total
954 precipitation error was also recorded to assess the overall error from each radar.

955

956 3 Results and discussion

957 3.1 Overall algorithm performance

958 To test the overall performance of each radar, it was necessary to determine the overall best
959 algorithm for each statistical measure. The best algorithm from each grouping of equations was
960 determined to have the lowest normalized standard error (NSE), indicating the best performance relative
961 to the gauge-recorded precipitation amount (Ryzhkov et al., 2005). This reduces the impact of bias
962 inherent within the dataset between warm/cool season, stratiform/convective events, and allows for
963 statistical measurements in spite of the (typical) non-Gaussian behavior of precipitation (Kleiber et al.,
964 2012; Alaya et al., 2017).

965 From the results obtained, the three R(Z), three R(DSMZ), and RREC algorithms displayed a
966 particular bias in favor of the R(Z)-Convective algorithm for all three radars with R(Z)-Stratiform
967 displaying similar performance (Figure 2a). This could be due, at least in part, to the near-equal stratiform
968 and convective precipitation regimes throughout 2014. Although errors generally increased as range
969 increased for KEAX and KLSX, the results were nebulous for KSGF. The lowest NSE values were,
970 typically, closest to each of the radars (between 0.4 and 0.8), with the notable exception of the closest
971 gauge to KSGF. In general, the RREC performed worst at the largest of ranges, potentially due to the
972 algorithm's ability to incorrectly assess the hydrometeors present (Cifelli et al., 2011; Yang et al. 2016).
973 Additionally, the poor performance by the R(DSMZ)-Tropical equation is due to the lack of tropical
974 precipitation within Central Missouri. Overall, the KDP-smoothed reflectivity fields (DSMZ) performed
975 worse than their counter-parts, resulting in over-prediction of precipitation and, thus, larger errors
976 (Simpson et al., 2016). Errors did not exceed 2.4 NSE units for any of these algorithms.

977 However, the performance of the KDP-smoothed KDP field (DKDP) performed better than the
978 original specific differential phase shift field (Figure 2b). For nearly all gauges for each of the 3 radars,
979 R(DKDP)4 performed the best, with NSE values ranging from 1.4 to 4.1. The range of NSE values were
980 largest at KEAX, while the spread was relatively small for KLSX and KSGF. In spite of this, the overall
981 spread of the performance of the 12 KDP algorithms varied greatly (average of 2 NSE units), exhibiting
982 the sensitivity of KDP estimates on OPE (Ryzhkov et al., 2005; Cunha et al., 2013). In general, the
983 NSSL-derived R(KDP) equations (i.e., equations 4-6) outperformed those from Bringi and Chandrasekar
984 (2001, equation 1), Brandes et al. (2002, equation 2), and Illingworth and Blackman (2002, equation 3).
985 Regardless, the magnitudes were all, approximately, more than 1 NSE unit than the performance of the
986 R(Z) algorithms.

987 The algorithms with the lowest NSE values were equations 7-11. For example, the overall lowest
988 NSE was at a distance of 130 km from KEAX (0.3), with no locations exceeding NSE values of 2.0
989 (Figure 2c). The large values at the closest location for KSGF (85 km, 1.3 – 1.9 NSE units), and the fifth

990 closest gauge to KLSX (135 km, 1.3 – 1.8 NSE units), Cook Station, were similar to the R(Z) and
991 R(DSMZ) results, indicating potential issues with reflectivity measurements. Additionally, these locations
992 were the closest in performance to the R(KDP) and R(DKDP) NSE values. Observations from this gauge
993 (Cook Station) indicated hail occurred during the evening of 01 August, for which KDP estimates would
994 be more ideal than Z for QPE (Ryzhkov et al. 2005; Kumjian 2013a; Cunha et al. 2015). In spite of this,
995 the overall spread in performance of the R(Z,ZDR) equations were less than the R(KDP) equations,
996 demonstrating the robust performance of R(Z,Z,ZDR) for QPE (Wang and Chandrasekar 2010; Seo et al.,
997 2015).

998 The R(ZDR,KDP) algorithms performed the worst, overall (Figure 2d). In spite of the differential
999 reflectivity being implemented, the overall NSE values increased in magnitude, exceeding 6 units for the
1000 second gauge analyzed by KEAX. Algorithms containing DKDP measurements performed better than
1001 simply KDP, demonstrating that even with the scaling behavior of ZDR, DKDP is superior to KDP
1002 estimates. This provides a potential solution to the noisy-ness that tends to be exhibited in the KDP field
1003 (Ruzanski and Chandrasekar 2012).

1004 Due to the overall NSE values obtained, for the remainder of the analyses, equation 11 (i.e.,
1005 R(Z,ZDR)5) and equation 13 (i.e., R(ZDR,KDP)2) will be utilized as the best and worst algorithms,
1006 respectively. Equations containing DZDR were not included in the following discussion due to the very
1007 large QPE errors for each radar.

1008

1009 3.2 KEAX

1010 The overall bias showed that there was a positive bias, peaking near 5.5 mm hr⁻¹ at the second
1011 gauge for KEAX, approximately 115 km from the radar for both the best and worst performing
1012 algorithms (Figure 3). This corresponds well with the spike in falsely detected precipitation recorded,
1013 which is canceled by the maximum in missed precipitation at the second distance of, approximately, 150

1014 km. The overall worst algorithm, equation 13, an R(ZDR,KDP) relationship, revealed a decreasing trend
1015 in bias as the distance from the radar increased. For example, a bias of 4 mm hr⁻¹ was observed at a
1016 distance of 75 km from the radar, whereas the bias reduced to 3 mm hr⁻¹ at distances near 175 km. This
1017 could be due, at least in part, to the algorithm's utilization of KDP which performs poorly in frozen
1018 (especially light) precipitation (Zrnich and Ryzhkov, 1996; Kumjian 2013a), causing the overestimation.
1019 Conversely, the algorithm with the lowest bias was an R(Z,ZDR) algorithm (equation 11). There was a
1020 maximum in the bias calculations while utilizing equation 11 near 120 km, similar to equation 13,
1021 however, there was a more pronounced minimum in the data near 150 km. Furthermore, it appears the
1022 data oscillates around a bias value of 0 mm hr⁻¹ when using equation 13. This could be due to ZDR's
1023 capability to respond to precipitation shape (Kumjian 2013a), which helps to scale the reflectivity portion
1024 of the rainfall estimation algorithm to a more accurate value (Seo et al., 2015). In general, the cool season
1025 displayed a larger magnitude of error in terms of bias for both algorithms.

1026 The normalized mean bias (NMB) reveals the same trend in values for bias but with an overall
1027 decrease in magnitude. It is important to note, however, that the algorithms that tend to perform the worst
1028 (e.g., algorithms containing KDP) result in anomalous range responses which would be due, at least in
1029 part, to a stronger response to precipitation type. This indicates that observations above the melting layer
1030 are dominant for which QPE's tend not to be calculated (Cifelli et al., 2011; Seo et al., 2015) but are
1031 important for regions devoid of adequate radar coverage (Ryzhkov et al., 2003; Simpson et al., 2016).

1032 The absolute bias and normalized standard error (NSE) shows the same maxima in the data at the
1033 second gauge (Brunswick) that was present in the bias data (6.2 mm hr⁻¹ and 5.6, respectively). However,
1034 a second maxima is located at the fifth gauge at, approximately, 150 km (Linneus) with values of 5.9 mm
1035 hr⁻¹ and 4.0, respectively. Bright-band issues are detected due, at least in part, to the increased missed
1036 precipitation amount (240 mm) at this particular distance for the R(ZDR,KDP) equation (i.e., worst
1037 performing algorithm). There was also a pronounced minimum in the absolute bias and NSE results at the
1038 fourth gauge for equations 11 and 13, 4.0 mm hr⁻¹ and 0.8 mm hr⁻¹, and 2.8 and 0.8, respectively,

1039 potentially indicating an idealized range of QPE for KEAX. Furthermore, the historical records at this
1040 particular gauge showed less issues (e.g., clogging) than any of the others analyzed by the KEAX radar.
1041 This highlights the importance of choosing ground-truth data, in particular tipping buckets which are
1042 prone to numerous errors (Ciach and Krajewski, 1999b).The largest contributions to the NSE and NMB
1043 were due to the warm season.

1044 The probability of detection (PoD) results indicate a large difference in algorithm choice for
1045 correctly detecting precipitation. The low PoD at, approximately 150 km, indicates overshooting of the
1046 beam. This is further evidenced by the MPA results, as about 225 mm of precipitation was missed by the
1047 radar at 150 km, whereas only 100 mm of precipitation was missed by the radar at the second gauge at
1048 120 km. Although equation 11, an R(Z,ZDR) algorithm was superior in terms of the bias, the same
1049 algorithm with a KDP-smoothed reflectivity value, R(DSMZ,ZDR) revealed the overall least amount of
1050 falsely missed precipitation (by 10 mm). However, the summation of the amount of precipitation falsely
1051 detected (PoFD) by KEAX showed a larger source of error than the MPA in terms of magnitude. For
1052 example, at the second (fifth) gauge, only 100 (225) mm of precipitation was missed by the radar, but
1053 over 700 (725) mm of precipitation was incorrectly estimated by the radar.

1054 Correlation coefficient (CC) values for any of the 9 stations analyzed by KEAX ranges from 0.02
1055 (Linneus, 151 km) to 0.93 for the cool season (St. Joseph, 115 km). The lowest R^2 were due to a
1056 combination of false alarms and misses. For example, the CC for the warm seasons at Sanborn (170 km)
1057 and Jefferson Farm (173 km) were 0.22 and 0.24, respectively, whereas when the instances of false
1058 alarms and misses were removed, increased to 0.48 and 0.52. Few locations (Brunswick, 114 km and
1059 Versailles, 129 km) saw little improvement in the CC values when only hits were analyzed (less than 0.1
1060 increase), indicating the mean absolute error (in terms of hits) contributed the largest portion of error.

1061

1062 3.3 KLSX

1063 Unlike the KEAX data, the gauges used for analyses for the KLSX radar span between 90 – 150
1064 km. Furthermore, 5 out of the 8 gauges were located within 10 km of range from one-another, near 140
1065 km from the radar, limiting the data available for analyses between 100 and 140 km (Figure 5).

1066 The bias and NMB both show a relatively modest peak in values near the second gauge of 5 mm ,
1067 which decreases to approximately 3.6 mm at the third gauge, 120 km from the radar. The worst
1068 performing algorithm, equation 13, was the same R(ZDR,KDP) relation as the worst KEAX bias and
1069 NMB data. Additionally, the overall trend of decreasing bias and NMB as distance from the radar
1070 increases was noted, presumably due to overshooting effects similar to the KEAX data. Furthermore, the
1071 overall non-biased results from the R(Z,ZDR) equation demonstrates its robust capabilities in OPE, in
1072 spite of its sensitivity to calibration (Zrnice et al., 2005; Bechini et al., 2008).

1073 The double maxima in the absolute bias graph are present as with the KEAX data, but are not as
1074 pronounced. For example, the absolute bias at 95 km and 140 km from KLSX were 5.9 mm and 1.1 mm ,
1075 and 4.9 mm and 1.4 mm for equations 13 and 11, respectively. Additionally, the overall minima in the
1076 absolute bias for both KEAX and KLSX are at, approximately, 125 km from the radar (3.9 mm hr⁻¹ and
1077 1.0 mm hr⁻¹, respectively, for equations 13 and 11). The relative distance from the radars are the same,
1078 where the two maxima for KEAX were at 115 and 150 km, while the maxima were at, approximately,
1079 100 and 140 km for KLSX. The overall best and worst performing algorithms at KLSX for the absolute
1080 bias and NSE were equations 11 and 13, the R(Z,ZDR) and R(ZDR,KDP) algorithms, respectively.

1081 The magnitude of error in terms of absolute bias, normalized mean bias, and normalized standard
1082 error, all showed a decreasing pattern as distance from KLSX increased. This was due, primarily, from a
1083 maximum in the false precipitation amount at 95 km from the radar. Historical notes at this location
1084 indicate frequent clogging of the rain gauge, either due to bugs or leaves. From a particular series of
1085 events spanning from 01 to 04 April and 01 to 03 August, 2014, over 130 mm of precipitation occurred
1086 during each period which was not captured by the gauge, resulting in a large amount of overall error.
1087 These results indicate the important of dual gauges in the same vicinity (Krajewski et al. 1998; Ciach and

1088 Krajewski 1999). Interestingly, the cool season displayed a larger NSE (5 % for R(ZDR,KDP))
1089 potentially due to the very low probability of detection (0.2) at this range of 118 km.

1090 One of the main differences between the KLSX and KEAX data was the decreased probability of
1091 detection at 120 km for KLSX, while there was an increased probability of detection for KEAX. In
1092 general, the PoD values were worse for KLSX when compared to KEAX. For example, equation 11 had
1093 no PoD values below 0.90, whereas no PoD values exceeded 0.84 for KLSX. There was also a slight
1094 trend of increasing PoD values as distance from the St. Louis radar increased and, at one point near 140
1095 km, the best algorithm, R(DSMZ) convective and the worst algorithm, KDP1, were not significantly
1096 different ($p < 0.10$). Additionally, the maxima in the PoD while utilizing KDP1 corresponds to a minima
1097 in the R(DSMZ) detection percentage, which is well correlated by the similarly valued MPA results.

1098 The missed precipitation amount (MPA) displayed the cool season contributed the most, whereas
1099 the warm season contributed the most amount of false precipitation amount. The R(Z,ZDR) equation only
1100 registered, on average, 25 mm of MPA and 160 mm of FPA, whereas the R(ZDR,KDP) equation was
1101 very dependent upon range. For example, the FPA from R(ZDR,KDP) decreased as range increased from
1102 the radar from a maximum of, approximately, 850 mm to 620 mm. However, the fifth-furthest gauge (137
1103 km from KLSX) displayed a sharp increase in the MPA for both cool seasons (above 100 mm).

1104

1105 3.4 KSGF

1106

1107 In spite that the KLSX and KEAX data strongly suggests false precipitation errors near 100 km in
1108 addition to bright-banding near 150 km from the radars, the KSGF results reveal an overall smooth
1109 decrease (increase) of error with range (Figure 7) for R(ZDR,KDP) and R(Z,ZDR), accordingly. One of
1110 the main reasons for this could be due to the fact that only 5 gauges were analyzed from KSGF (the
1111 fewest of the 3 radars analyzed), smoothing the overall trend lines.

1112 The bias remained relatively constant near -0.3 mm for R(Z,ZDR), whereas the bias exhibited a
1113 sharp decrease from 4 mm to 2.7 mm over a distance of, approximately, 100 km. In general, the cool
1114 season displayed the lower of bias magnitudes when compared to the warm season, similar to the KEAX
1115 results. This may be due, at least in part, to the low PoFD values for the warm season close to the KSGF
1116 radar.

1117 Similar to the bias, the absolute bias for R(Z,ZDR) was constant at all ranges (near 1 mm)
1118 whereas the R(ZDR,KDP) equation decreased from 5.2 mm to 3.8 mm. This is potentially due to the low
1119 cool season PoD values (below 0.6), while the warm season R(ZDR,KDP) values (near 0.8) remained
1120 constant. A larger contribution from more correctly detected precipitation in addition to the decreasing
1121 trends in the NMB and NSE would result in a lower absolute bias.

1122 The closest location (90 km) typically displayed the largest errors for the R(ZDR,KDP) equation,
1123 and then decreased in error magnitude as range increased. In spite of this, the PoFD results indicate both
1124 algorithms increased in PoFD values as range increased, with the warm season typically dominating,
1125 particularly due to the large convective clouds dominate in the warm season. False detection values as
1126 low as 0.01 for the cool season while utilizing R(Z,ZDR) were observed at distances near 100 km and 140
1127 km from the radar.

1128 Normalized standard error values increased from 0.7 % at a distance of 105 km to 1.8 % at a
1129 distance of 185 km for R(Z,ZDR). Large NSE values for the warm season (7.5 %) were calculated for
1130 R(ZDR,KDP) which decreased to 3.8 % at 185 km from the radar. Furthermore, this was the only
1131 instance when the warm season was less than the cool season in terms of NSE. Otherwise, the overall
1132 NSE decreased from 5 % to 3.9 % for R(ZDR,KDP). The NMB followed a similar trend for the KDP-
1133 containing algorithm, with a noticeable exception at the second gauge (105 km from KSGF), where the
1134 overall NSE was closer to the warm than cool season. This is due to the low PoFD values at this location,
1135 in addition to a smaller difference between the two algorithm's FPA measurements.

1136 The MPA results, unlike for KEAX and KLSX, displayed a larger range of performance between
1137 seasons. However, the warm season still exhibited the overall best performance in terms of MPA, yet
1138 contributed the most to the FPA for both R(Z,ZDR) and R(ZDR,KDP). In spite of the MPA typically
1139 increasing as range increased, the FPA was more nebulous. For example, the second gauge (105 km from
1140 KSGF) had the overall lowest NSE (0.8 %), MPA (15 mm), and FPA (95 mm) for R(Z,ZDR). The third-
1141 furthest location (142 km) resulted in slightly larger errors, overall, while the fourth-furthest location had
1142 errors similar to the second gauge (105 km). Then, at the furthest tipping bucket location (185 km), NSE
1143 values increased, whereas FPA and MPA decreased. Therefore, the furthest location's errors are due,
1144 primarily, from discrepancies between precipitation magnitude between the gauge and radar.

1145 Excluding Versailles (142 km from KSGF), the cool season exhibited larger R² values in
1146 comparison to the cool season (Figure 8). Furthermore, CC values exceeded 0.9 when false alarms and
1147 misses were excluded from Mt. Grove (101 km) and was 0.84 when included. Otherwise, the other four
1148 stations analyzed by the Springfield radar displayed many counts of false alarms and misses, leading to
1149 low R² values.

1150 Due to the relatively large ranges from the Springfield (KSGF) radar, most of the correlation
1151 coefficient values were low in comparison to either KLSX or KEAX. For the warm (cool) season without
1152 false alarms and misses, R² values ranged from 0.44 (0.38) and 0.34 (0.36) for KLSX and KSGF,
1153 respectively, at Cook Station (119 and 185 km). Similarly, the CC values ranged from 0.61 (0.71) to 0.42
1154 (0.56) at Green Ridge (76 and 154 km) for KEAX and KSGF, accordingly.

1155 4 Conclusions

1156 Dual-polarization technology was implemented to the National Weather Service Next Generation
1157 Radar network in the Spring of 2012 to, primarily, improve quantitative precipitation estimation and
1158 hydrometeor classification. The current study observed over 300 hours of precipitation data with three
1159

1160 separate radars in Missouri using 55 algorithms including the three conventional R(Z) radar rain-rate
1161 estimation algorithms (stratiform, convective, and tropical) along with a myriad of R(KDP), R(Z,ZDR),
1162 and R(ZDR,KDP) algorithms which can be found in Ryzhkov et al. (2005). Additionally, a KDP-
1163 smoothing field of reflectivity, differential reflectivity, and the specific differential phase shift (DSMZ,
1164 DZDR, and DKDP, respectively) were measured and used for analyses. Unlike previous studies, the
1165 current work emphasizes the amount of precipitation correctly and incorrectly estimated by the radar in
1166 comparison to the terrestrial based precipitation gauges through measurements of the missed and false
1167 precipitation amount.

1168 For all three radars, Kansas City, St. Louis, and Springfield, MO (KEAX, KLSX, and KSGF,
1169 respectively), the majority of precipitation error (over 60%) was contributed by the amount of
1170 precipitation falsely detection by the radar (up to 725 mm), while 20% was due to the radar missing the
1171 precipitation (up to 225 mm) for KEAX. Similar magnitudes of error were reported for KLSX and KSGF,
1172 with an overall error in precipitation for each radar ranging between 250 mm for the best performing of
1173 the 55 algorithms, equation 11 (an R(Z,ZDR) algorithm), and up to 2000 mm for the worst performing
1174 algorithms, R(ZDR,KDP) equation 13. The R(Z,ZDR) equation (an NSSL algorithm) was determined to
1175 be the most robust due to it registering the lowest NSE. These values of false precipitation amount and
1176 missed precipitation amount generally increased as range from the radar increased.

1177 Most algorithms showed a degradation in the normalized standard error with range. In particular,
1178 the KDP-smoothed equations displayed larger biases and NSE values than their non-KDP counterparts,
1179 with the exception of R(KDP) algorithms themselves. Some larger errors were recorded at gauge
1180 locations close to the radar, potentially due to bright-banding effects which were determined to be due to
1181 the large false precipitation amount analyzed at these locations.

1182 The data was divided into summer (May – October) and winter (November – April; 59 and 41%
1183 of the entire data, respectively). Despite the winter data contributing less than the summertime data, it
1184 accounted for 20% of the overall MPA, and 40% to the overall PoFD. The R^2 values were less during the

1185 winter in comparison to the warm season primarily due to the smaller magnitude of precipitation that
1186 occurred. Furthermore, CC values increased by as much as 0.4 when instances of hits and misses were
1187 removed from the analyses, resulting in the warm season to outperform the cool season CC values at
1188 particularly short ranges from the radar.

1189 These results aid in our understanding in the possibilities for hydrometeorological studies. Nearly
1190 50% of the 300 hours where precipitation occurred analyzed for the study consisted of either falsely
1191 estimated precipitation by the radar, or missed by the radar. Furthermore, these errors accumulate
1192 between 500 to 2,000 mm of precipitation depending on the algorithms chosen. Although the overall
1193 performance increased when false alarms and misses were removed, correlation coefficient values still,
1194 typically, remained below 0.50 at ranges beyond 130 km.

1195 Furthermore, results demonstrate the issues with analyzing QPE from a single gauge, explaining
1196 why the Community Collaborative Rain, Hail, and Snow Network (Kelsch 1998; Cifelli et al., 2005;
1197 Reges et al., 2016) or other densely-gauged networks (e.g., the Hydrometeorological Automated Data
1198 System, HADS, Meteorological Assimilation Data Ingest System, MADIS) tends to be more utilized
1199 since results have shown that measurements or quality controlled-techniques made by these organizations,
1200 especially CoCoRaHS, are significantly more accurate than rain gauges (Simpson et al., 2017), especially
1201 for convective events (Moon et al. 2009).

1202
1203 **Author Contribution.** N. Fox designed the experiment and provided feedback while M. Simpson carried
1204 out the calculations and wrote the manuscript.

1205 **Acknowledgements.** This material is based upon work supported by the National Science Foundation
1206 under Award Number IIA-1355406. Any opinions, findings, and conclusions or recommendations
1207 expressed in this material are those of the authors and do not necessarily reflect the views of the National
1208 Science Foundation.

1209

1210

References

1211

Alaya, M.A., Ourda, T.B.M.J., Chebana, F.: Non-Gaussian spatiotemporal simulation of multisite

1212

precipitation: Downscaling framework. *Climate Dynamics*, 2017. doi:

1213

<https://doi.org/10.1007/s00382-017-3578-0>.

1214

Anagnostou, M.N., Anagnostou, E.N., Vulpiani, G., Montopoli, M., Marzano, F.S., Vivekanandan, J.:

1215

Evaluation of X-band polarimetric-radar estimates of drop-size distributions from coincident S-

1216

band polarimetric estimated and measured raindrop spectra. *IEEE Transactions on Geoscience*

1217

and Remote Sensing, 46, 3067-3075, 2008.

1218

Bechini, R., Baldini, L., Cremonini, R., Gorgucci, E.: Differential reflectivity calibration for operational

1219

radars. *Journal of Atmospheric and Oceanic Technology*, 25, 1542-1555, 2009.

1220

Berne, A. and Uijlenhoet, R.: A stochastic model of range profiles of raindrop size distributions:

1221

application to radar attenuation correction, *Geophysical Research Letters*, 32, 2005, doi:

1222

<https://doi.org/10.1029/2004GL021899>.

1223

Berne, A. and Krajewski, W.F.: Radar for hydrology: Unfulfilled promise or unrecognized potential?

1224

Advances in Water Resources, 51, 357-366, 2013.

1225

Bringi, V.N. and Chandrasekar, V.: Polarimetric Doppler weather radar, principles and applications.

1226

Cambridge University Press: Cambridge, UK, 636, 2001.

1227

Brandes, E.A., Zhang, G., Vivekanandan, J.: Experiments in rainfall estimation with a polarimetric radar in

1228

a subtropical environment, *Journal of Applied Meteorology*, 41, 674–685, 2002.

1229

Brandes, E.A., Zhang, G., Vivekanandan, J.: Drop size distribution retrieval with polarimetric radar: model

1230

and application, *Journal of Applied Meteorology*, 43, 461-475, 2004.

1231 [Chai, T., Draxler, R.R.: Root mean square error \(RMSE\) or mean absolute error \(MAE\)? – Arguments](#)
1232 [against avoiding RMSE in the literature, Geoscientific Model Development, 7, 1247-1250, 2014.](#)

1233 [Ciach, G.J., Krajewski, W.F.: On the estimation of radar rainfall error variance. Advances in Water](#)
1234 [Resources, 22, 585-595, 1999a.](#)

1235 [Ciach, G.J. and Krajewski, W.F.: Radar-rainage comparisons under observational uncertainties. Journal](#)
1236 [of Applied Meteorology, 38, 1519-1525, 1999b.](#)

1237 [Ciach, G.J.: Local random errors in tipping-bucket rain gauge measurements. Journal of Atmospheric and](#)
1238 [Oceanic Technology, 20, 752-759, 2002.](#)

1239 [Cifelli, R., Doesken, N., Kennedy, P., Carey, L.S., Rutledge, S.A., Gimmestad, C., Depue, T.: The community](#)
1240 [collaborative rain, hail, and snow network: Informal education for scientists and citizens.](#)
1241 [Bulletin of the American Meteorological Society, 86, 1069-1077, 2005.](#)

1242 [Cunha, L.K., Smith, J.A., Baeck, M.L., Krajewski, W.F.: An early performance of the NEXRAD dual-](#)
1243 [polarization radar rainfall estimates for urban flood applications. Weather and Forecasting, 28,](#)
1244 [1478-1497, 2013.](#)

1245 [Cunha, L.K., Smith, J.A., Krajewski, W.F., Baeck, M.L., Seo, B.: NEXRAD NWS polarimetric precipitation](#)
1246 [product evaluation for IFloods. Journal of Hydrometeorology, 16, 1676-1699, 2015.](#)

1247 [Delrieu, G., Andrieu, H., Creutin, J.D.: Quantification of path-integrated attenuation for X- and C-band](#)
1248 [weather radar systems operating in Mediterranean heavy rainfall. Journal of Applied](#)
1249 [Meteorology, 39, 840-850, 2000.](#)

1250 [Fabry, F., Bellon, A., Duncan, M.R., Austin, G.L.: High resolution rainfall measurements by radar for very](#)
1251 [small basins: the sampling problem reexamined. Journal of Hydrology, 161, 415-428, 1994.](#)

1252 [Fairman, J.G., Schultz, D.M., Kirschbaum, D.J., Gray, S.L., Barrett, A.I.: A radar-based rainfall climatology](#)
1253 [of Great Britain and Ireland. *Weather*, 70, 153-158, 2012. doi:](#)
1254 [https://doi.org/10.1002/wea.2486.](https://doi.org/10.1002/wea.2486)

1255 [Gamache, J.F. and Houze, R.A.: Mesoscale air motions associated with a tropical squall line. *Monthly*](#)
1256 [Weather Review](#), 110, 118–135, 1982.

1257 [Giangrande, S.E. and Ryzhkov, A.V.: Estimation of rainfall based on the results of polarimetric echo](#)
1258 [classification. *Journal of Applied Meteorology*, 47, 2445-2460, 2008.](#)

1259 [Gorgucci, E., Scarchilli, G., Chandrasekar, V.: Calibration of radars using polarimetric techniques. *IEEE*](#)
1260 [Transactions in Geoscience and Remote Sensing](#), 30, 853-858, 1992. [Gorgucci, E., Scarschilli, G.,](#)
1261 [Chandrasekar, V., Bringi, V.N.: Measurement of mean raindrop shape from polarimetric radar](#)
1262 [observations. *Journal of the Atmospheric Sciences*, 57, 3406-3413, 2000.](#)

1263 [Gorgucci, E., Baldini, L., Chandrasekar, V.: What is the shape of a raindrop? An answer from radar](#)
1264 [measurements. *Journal of the Atmospheric Sciences*, 63, 3033-3044, 2006.](#)

1265 [Goudenhoofdt, E., Delobbe, L.: Long-term evaluation of radar QPE using VPR correction and radar-gauge](#)
1266 [merging. *International Association of Hydrological Sciences Publications*, 351, 249-254, 2012.](#)

1267 [Goudenhoofdt, E., Delobbe, L.: Generation and verification of rainfall estimates from 10-yr volumetric](#)
1268 [weather radar measurements. *Journal of Hydrometeorology*, 133, 1191-1204, 2016.](#)

1269 [Gourley, J.J., Giangrande, S.E., Hong, Y., Flamig, Z., Schuur, T., Vrugt, J.: Impacts of polarimetric radar](#)
1270 [observations on hydrologic simulation. *Journal of Hydrometeorology*, 11, 781-796, 2010.](#)

1271 [Habib, E., Krajewski, W.F., Nespor, V., Kruger, A.: Numerical simulation studies of rain gauge data](#)
1272 [correction due to wind effect. *Journal of Geophysical Research*, 104, 723–734, 1999.](#)

1273 [Habib, E., Krajewski, W.F., Kruger, A.: Sampling errors of tipping-bucket rain gauge measurements.](#)
1274 [Journal of Hydrological Engineering, 6, 159–166, 2001.](#)

1275 [Haylock, M.R., Hofstra, N., Klein Tank, A.M.G., Klok, E.J., Jones, P.D., New, M.: A European daily high-](#)
1276 [resolution gridded data set of surface temperature and precipitation for 1950-2006. Journal of](#)
1277 [Geophysical Research, 113, 2008. doi: <https://doi.org/10.1029/2008JD010201>](#)

1278 [Holleman, I., Huuskonen, A., Gill, R., Tabary, P.: Operational monitoring of radar differential reflectivity](#)
1279 [using the sun. Journal of Atmospheric and Oceanic Technology, 27, 881-887, 2010.](#)

1280 [Hubbert, J.C.: Differential reflectivity calibration and antenna temperature. Journal of Atmospheric and](#)
1281 [Oceanic Technology, 34, 1885-1906, 2017.](#)

1282 [Illingworth, A., Blackman, T.A.: The need to represent raindrop size spectra as normalized gamma](#)
1283 [distributions for the interpretation of polarization radar observations. Journal of Applied](#)
1284 [Meteorology, 41, 286-297, 2002.](#)

1285 [Kelsch, M.: The Fort Collins flash flood: Exceptional rainfall and urban runoff. Preprints, 19th Conference](#)
1286 [on severe local storms, Minneapolis, MN, American Meteorological Society, 404-407, 1998.](#)

1287 [Kitchen, M. and Blackall, M.: Representativeness errors in comparisons between radar and gauge](#)
1288 [measurements of rainfall. Journal of Hydrology, 134, 13–33, 1992.](#)

1289 [Kleiber, W., Katz, R.W., Rajagopalan, B.: Daily spatiotemporal precipitation simulation using latent and](#)
1290 [transformed Gaussian processes. Water Resources Research, 48, 2012. doi:](#)
1291 [https://doi.org/10.1029/2011WR011105.](https://doi.org/10.1029/2011WR011105)[Kessinger, C., Ellis, S., Van Andel, J.: The radar echo](#)
1292 [classifier: a fuzzy logic algorithm for the WSR-88D. 19th Conf. on Inter. Inf. Proc. Sys. \(IIPS\) for](#)
1293 [Meteor., Ocean., and Hydr., Amer. Meteor. Soc., Long Beach, CA, 2003.](#)

1294 [Kitchen, M. and Jackson, P.M.: Weather radar performance at long range – simulated and observed.](#)
1295 [Journal of Applied Meteorology, 32, 975-985, 1993.](#)

1296 [Krajewski, W.F., Kruger, A., Nespor, V.: Experimental and numerical studies of small-scale rainfall](#)
1297 [measurements and variability. Water Science and Technology, 37, 131-138.](#)

1298 [Kumjian, M.R.: Principles and applications of dual-polarization weather radar. Part 1: Description of the](#)
1299 [polarimetric radar variables. Journal of Operational Meteorology, 1, 226-242, 2013a.](#)

1300 [Kumjian, M.R.: Principles and applications of dual-polarization weather radar. Part 2: Warm and cold](#)
1301 [season applications. Journal of Operational Meteorology, 1, 243-264, 2013b.](#)

1302 [Kumjian, M.R.: Principles and applications of dual-polarization weather radar. Part 3: Artifacts. Journal of](#)
1303 [Operational Meteorology, 1, 265-274, 2013c.](#)

1304 [Lakshmanan, V., Smith, T., Stumpf, G., Hondl, K.: The warning decision support system—integrated](#)
1305 [information. Weather and Forecasting, 22, 596–612, 2007a.](#)

1306 [Lakshmanan, V., Fritz, A., Smith, T., Hondl, K., Stumpf, G.: An automated technique to quality control](#)
1307 [radar reflectivity data. Journal of Applied Meteorology and Climatology, 46, 288-305, 2007b.](#)

1308 [Lakshmanan, V., Zhang, J., Howard, K.: A technique to censor biological echoes in radar reflectivity data.](#)
1309 [Journal of Applied Meteorology and Climatology, 49, 453-462, 2010.](#)

1310 [Lakshmanan, V., Karstens, C., Krause, J., Tang, L.: Quality control of weather radar data using](#)
1311 [polarimetric variables. Journal of Atmospheric and Oceanic Technology, 31, 1234-1249, 2014.](#)

1312 [Moon, J.T., Guinan, P.E., Snider, D.J., Lupo, A.R.: CoCoRaHS in Missouri: Four years later, the importance](#)
1313 [of observations. Transactions of the Missouri Academy of Science, 43, 7-18, 2009.](#)

1314 [Park, H.S., Ryzhkov, A.V., Zrnice, D.S.: The hydrometeor classification algorithm for the polarimetric WSR-](#)
1315 [88DL Description and application to an MCS. Weather and Forecasting, 24, 730-748, 2009.](#)

1316 [Reges, H.W., Doesken, N., Turner, J., Newman, N., Bergantino, A., Schwalbe, Z.: CoCoRaHS: The](#)
1317 [evolution and accomplishments of a volunteer rain gauge network. Bulletin of the American](#)
1318 [Meteorological Society, 97, 1831-1846, 2016.](#)

1319 [Ruzanski, E., Chandrasekar, V.: Nowcasting rainfall fields derived from specific differential phase. Journal](#)
1320 [of Applied Meteorology and Climatology, 51, 1950-1959, 2012.](#)

1321 [Ryzhkov, A.V., Giangrande, S., Schurr, T.: Rainfall measurements with the polarimetric WSR-88D radar.](#)
1322 [National Severe Storms Laboratory Rep. Norman: OK, 98, 2003.](#)

1323 [Ryzhkov, A.V., Giangrande, S., Schurr, T.: Rainfall estimation with a polarimetric prototype of WSR-88D.](#)
1324 [Journal of Applied Meteorology, 44, 502-515, 2005.](#)

1325 [Scarchilli, G., Gorgucci, E., Chandrasekar, V., Dobaie, A.: Self-consistency of polarization diversity](#)
1326 [measurement of rainfall. IEEE Transactions in Geoscience and Remote Sensing, 34, 22-26, 1996.](#)

1327 [Shucksmith, P.E., Sutherland-Stacey, L., Austin, G.L.: The spatial and temporal sampling errors inherent](#)
1328 [in low resolution radar estimates of rainfall. Meteorological Applications, 18, 354-360, 2011.](#)

1329 [Simpson, M.J., Hubbart, J.A., Fox, N.I.: Ground truthed performance of single and dual-polarized radar](#)
1330 [rain rates at large ranges. Hydrological Processes, 30, 3692-3703, 2016.](#)

1331 [Simpson, M.J., Hirsch, A., Grempler, K., Lupo, A.R.: The importance of choosing precipitation datasets.](#)
1332 [Hydrological Processes, 1-13. doi: <https://doi.org/10.1002/hyp.11381>.](#)

1333 [Seo, B.-C., Dolan, B., Krajewski, W., Rutledge, S.A., Petersen, W.: Comparison of single- and dual-](#)
1334 [polarization-based rainfall estimates using NEXRAD data for the NASA Iowa Flood Studies](#)
1335 [project. Journal of Hydrometeorology, 16, 1658-1675, 2015.](#)

1336 [Smith, J.A., Seo, D.J., Baeck, M.L., Hudlow, M.D.: An intercomparison study of NEXRAD precipitation](#)
1337 [estimates. Water Resources Research, 32, 2035-2045, 1996.](#)

1338 [Straka, J.M., Zrnica, D.S., Ryzhkov, A.V.: Bulk hydrometeor classification and quantification using](#)
1339 [polarimetric radar data: Synthesis of relations. Journal of Applied Meteorology, 39, 1341-1372,](#)
1340 [2000.](#)

1341 [Yang, L., Yang, Y., Liu, P., Wang, L.: Radar-derived quantitative precipitation estimation based on](#)
1342 [precipitation classification. Advances in Meteorology, 2016, 2016. doi:](#)
1343 [https://doi.org/10.1155/2016/2457489.](https://doi.org/10.1155/2016/2457489)

1344 [Zhang, G., Vivekanandan, J., Brandes, E.A.: A method for estimating rain rate and drop size distribution](#)
1345 [from polarimetric radar measurements. IEEE Transactions on Geoscience and Remote Sensing,](#)
1346 [39, 830-841, 2001.](#)

1347 [Zhang, J., Youcun, Q.: A real-time algorithm for the correction of brightband effects in radar-derived](#)
1348 [QPE. Journal of Hydrometeorology, 11, 1157-1171.](#)

1349 [Zhang, J., Langston, C., Howard, K.: Brightband identification based on vertical profiles of reflectivity](#)
1350 [from the WSR-88D. Journal of Atmospheric and Oceanic Technology, 25, 1859-1872.](#)

1351 [Zrnica, D.S., Ryzhkov, A.V.: Advantages of rain measurements using specific differential phase. Journal of](#)
1352 [Atmosphere and Oceanic Technology, 13, 454-464, 1996.](#)

1353 [Zrnica, D.S., Ryzhkov, A.V.: Polarimetry for weather surveillance radars. Bulletin of American](#)
1354 [Meteorological Society, 80, 389-406, 1999.](#)

1355 [Zrnica, D.S., Melnikov, V.M., Carter, J.K.: Calibrating differential reflectivity on the WSR-88D. Journal of](#)
1356 [Atmospheric and Oceanic Technology, 23, 944-951, 2005.](#)

1357

1358

1359
1360
1361
1362
1363
1364
1365
1366

1367 Table 1. Terrestrial-based precipitation gauge locations used for the study in addition to the National
1368 Weather Service Radars Springfield, MO (KSGF), Kansas City, MO (KEAX), and St. Louis, MO
1369 (KLSX) used in conjunction with each gauge.

Gauge Location	Latitude (°N)	Longitude (°W)	Radar(s) Used
Bradford	38.897236	-92.218070	KLSX, KEAX
Brunswick	39.412667	-93.196500	KEAX
Capen Park	38.929237	-92.321297	KLSX, KEAX
Cook Station	37.797945	-91.429645	KLSX, KSGF
Green Ridge	38.621147	-93.416652	KEAX, KSGF
Jefferson Farm	38.906992	-92.269976	KLSX, KEAX
Lamar	37.493366	-94.318185	KSGF
Linneus	39.856919	-93.149726	KEAX

Monroe City	39.635314	-91.725370	KLSX
Mountain Grove	37.153865	-92.268831	KSGF
Sanborn Field	38.942301	-92.320395	KLSX, KEAX
St. Joseph	39.757821	-94.794567	KEAX
Vandalia	39.302300	-91.513000	KLSX
Versailles	38.434700	-92.853733	KEAX, KSGF
Williamsburg	38.907350	-91.734210	KLSX

1370

1371

1372

1373

1374

1375 Table 2. List of single- and dual-polarimetric algorithms used for radar rainfall estimates.

$R(Z) = aZ^b$			
Precipitation type	a	b	c
Stratiform	200	1.6	-
Convective	300	1.4	-
Tropical	250	1.2	-
$R(KDP) = a KDP ^b \text{sign}(KDP)$			
Algorithm number			
1	50.7	0.85	-
2	54.3	0.81	-
3	51.6	0.71	-

4	44.0	0.82	-
5	50.3	0.81	-
6	47.3	0.79	-

$$R(Z, ZDR) = aZ^b ZDR^c$$

Algorithm number			
7	6.70×10^{-3}	0.927	-3.43
8	7.46×10^{-3}	0.945	-4.76
9	1.42×10^{-2}	0.770	-1.67
10	1.59×10^{-2}	0.737	-1.03
11	1.44×10^{-2}	0.761	-1.51

$$R(ZDR, KDP) = a |KDP|^b ZDR^c \text{sign}(KDP)$$

Algorithm number			
12	90.8	0.930	-1.69
13	136	0.968	-2.86
14	52.9	0.852	-0.53
15	63.3	0.851	-0.72

1376

1377

1378

1379

1380

1381

1382

1383

1384

1385

1386

1387

1388

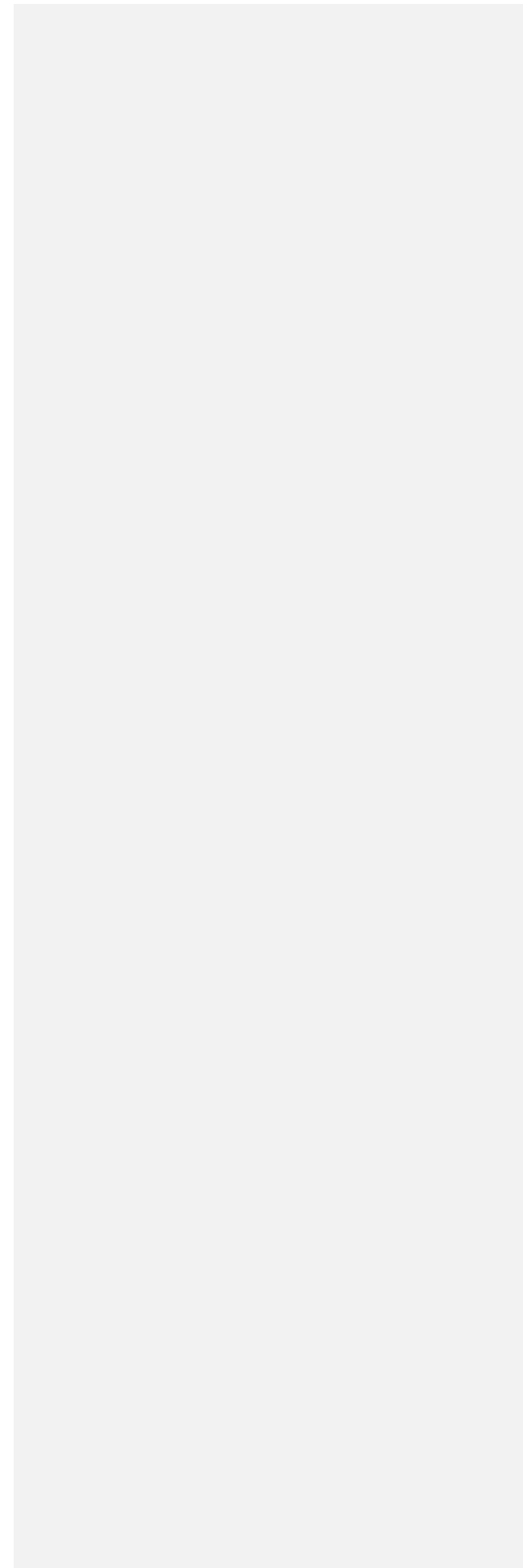
1389

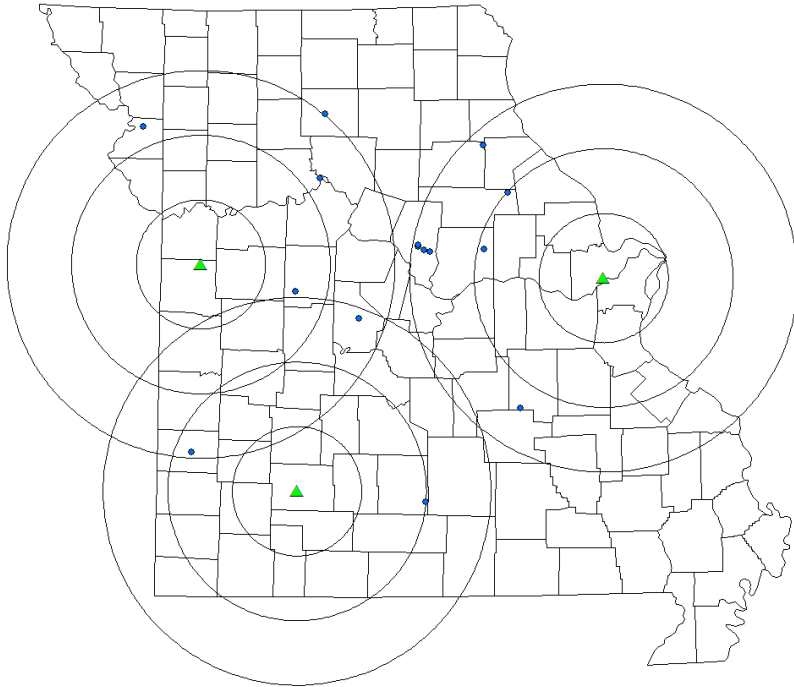
1390

1391

1392

1393 **Figures**





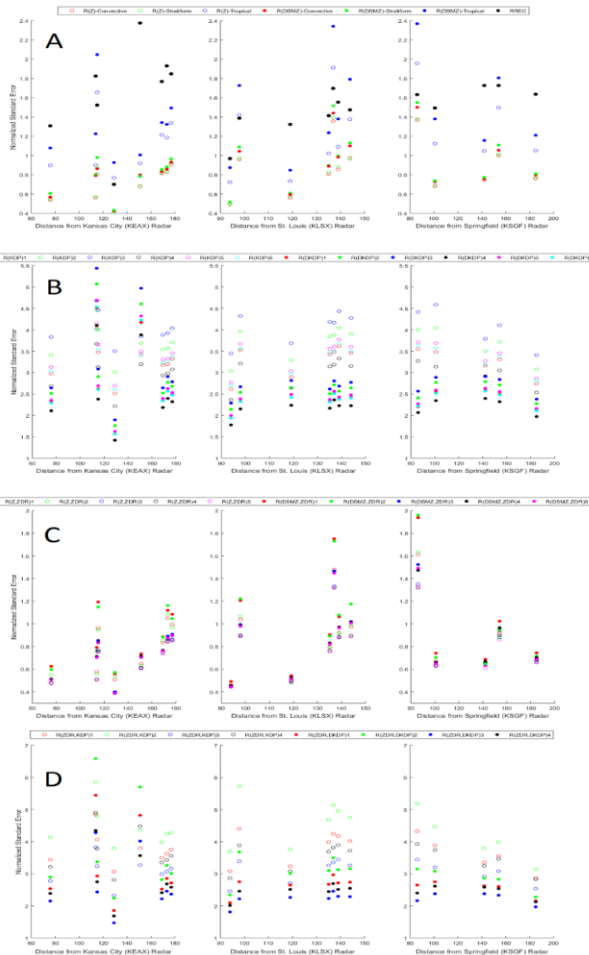
1394

1395 Figure 1. Study location (Missouri) with St. Louis (KLSX), Kansas City (KEAX), and Springfield
1396 (KSGF), MO radars (triangles) overlaid with 50-, 100-, and 150-km range rings in addition to the 15
1397 terrestrial-based precipitation gauges utilized as ground-truthed data.

1398

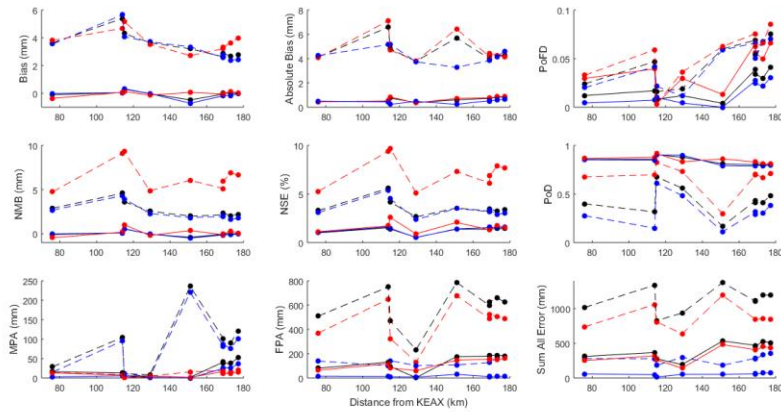
1399

1400



1401

1402 Figure 2. Normalized standard error values for the overall performance of the a) 3 R(Z), 3 R(DSMZ),
 1403 and RREC algorithms, b) 6 R(KDP) and 6 R(DKDP) algorithms (equations 1-6 from Table 2), c)
 1404 R(Z,ZDR) and 5 R(DSMZ,ZDR) algorithms (equations 7-11 from Table 2), and d) 4 R(ZDR,KDP)
 1405 and 4 R(ZDR,DKDP) algorithms (equations 12-15 from Table 2) for the three radars utilized for the
 1406 current study.



1407

1408 Figure 3. Values of analyses from the Kansas City (KEAX) radar. Dashed lines and points represent
 1409 the analyses of the worst-performing algorithm (R(ZDR,KDP)) while the solid lines and points
 1410 represent the analyses of the best-performing algorithm (R(Z,ZDR)). Red, blue, and black colors
 1411 represent analyses conducted during the warm and cool seasons, and overall, respectively.

1412

1413

1414

1415

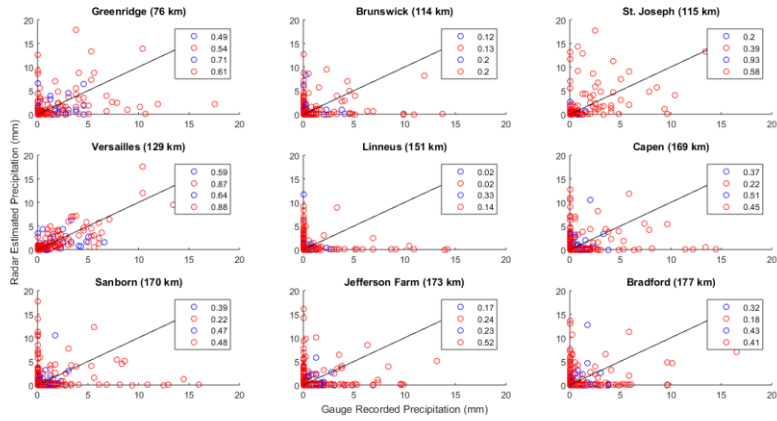
1416

1417

1418

1419

1420



1421

1422 Figure 4. Correlation coefficient values for the 9 locations analyzed by the Kansas City (KEAX) radar

1423 with the R(Z,ZDR) NSSL equation. Blue and red scatter points represent the cool and warm season

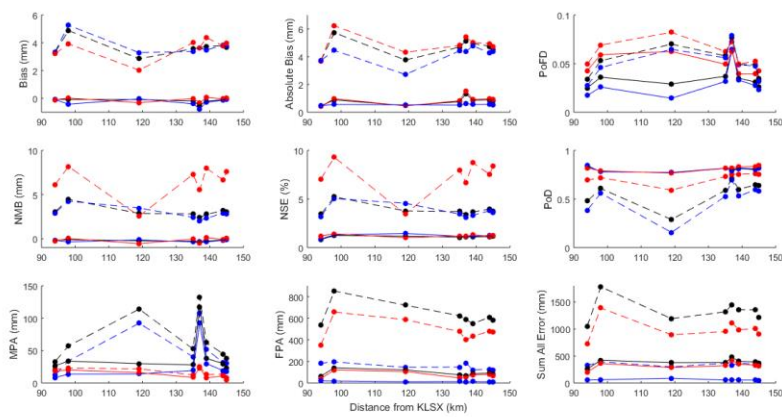
1424 data, respectively. The top two numbers on each plot indicate the overall R^2 value, whereas the

1425 bottom two numbers represent the R^2 when false alarms and misses are removed.

1426

1427

1428



1429

1430 Figure 5. Values of analyses from the St. Louis (KLSX) radar. Dashed lines and points represent the
 1431 analyses of the worst-performing algorithm (R(ZDR,KDP)) while the solid lines and points represent
 1432 the analyses of the best-performing algorithm (R(Z,ZDR)). Red, blue, and black colors represent
 1433 analyses conducted during the warm and cool seasons, and overall, respectively.

1434

1435

1436

1437

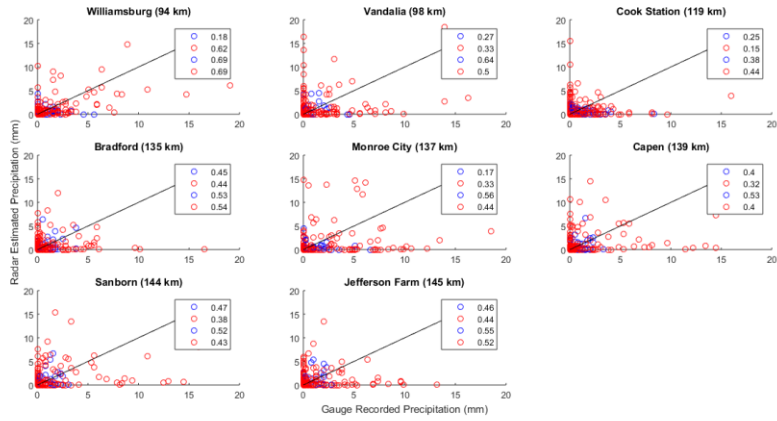
1438

1439

1440

1441

1442

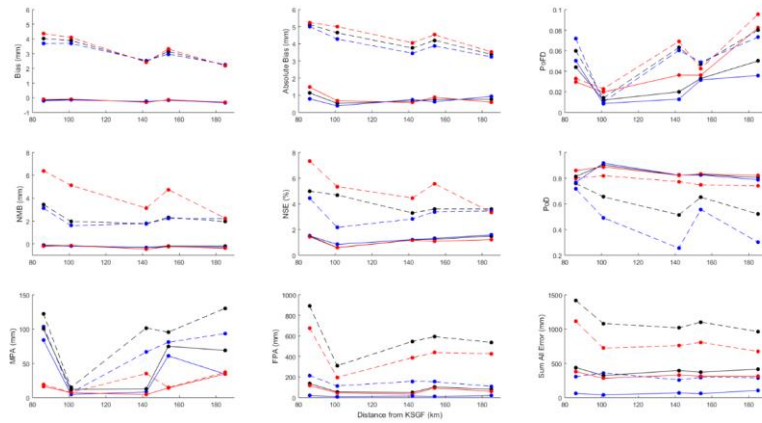


1443

1444 Figure 6. Correlation coefficient values for the 8 locations analyzed by the St. Louis (KLSX) radar
 1445 with the R(Z,ZDR) NSSL equation. Blue and red scatter points represent the cool and warm season
 1446 data, respectively. The top two numbers on each plot indicate the overall R² value, whereas the
 1447 bottom two numbers represent the R² when false alarms and misses are removed.

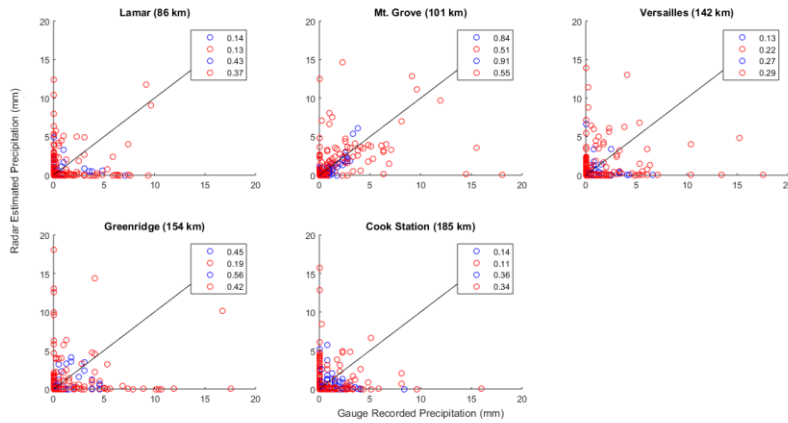
1448

1449



1450
 1451 Figure 7. Values of analyses from the Springfield (KSGF) radar. Dashed lines and points represent
 1452 the analyses of the worst-performing algorithm (R(ZDR,KDP)) while the solid lines and points
 1453 represent the analyses of the best-performing algorithm (R(Z,ZDR)). Red, blue, and black colors
 1454 represent analyses conducted during the warm and cool seasons, and overall, respectively.

1455
 1456
 1457
 1458
 1459
 1460
 1461
 1462
 1463



1464

1465 Figure 8. Correlation coefficient values for the 5 locations analyzed by the Springfield (KSGF) radar with
 1466 the R(Z,ZDR) NSSL equation. Blue and red scatter points represent the cool and warm season data,
 1467 respectively. The top two numbers on each plot indicate the overall R^2 value, whereas the bottom two
 1468 numbers represent the R^2 when false alarms and misses are removed.

1469